One Earth

Article

Mapping 25 years of global soil salinity: Hydrothermal conditions drive widespread desalinization amid regional salinization hotspots

Graphical abstract

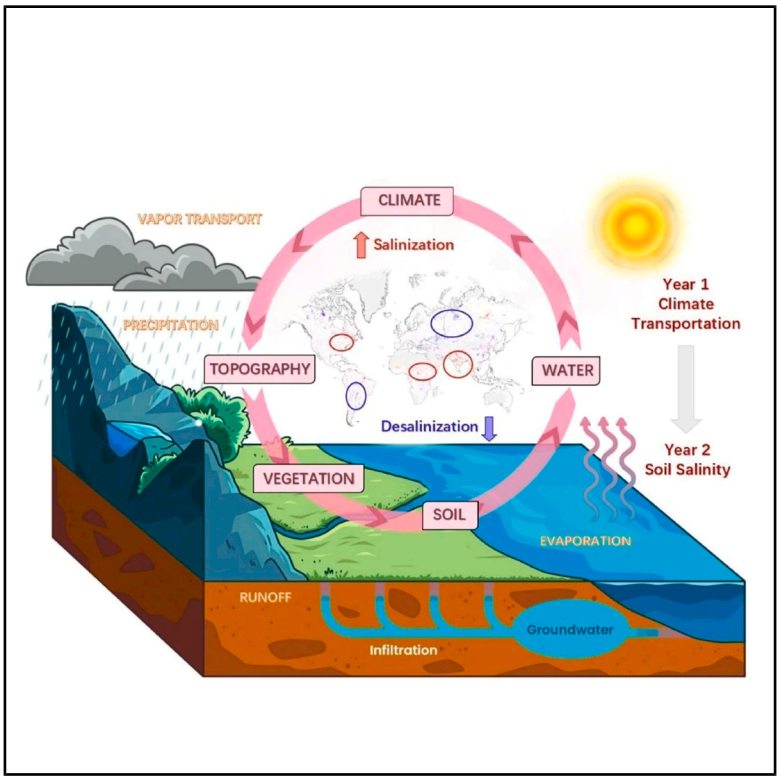

Authors

Nan Wang, Dietian Yu, Songchao Chen, ..., Frederic Frappart, Asim Biswas, Zhou Shi

Correspondence

shizhou@zju.edu.cn

In brief

Global soil salinity dynamics from 2000 to 2024 are revealed at 1-km resolution using machine learning. While a widespread desalinization trend is observed, concerning salinization hotspots emerge in tropical agricultural zones and high-latitude regions. Soil evaporation is identified as the dominant driver, providing scientific guidance for targeted management strategies.

Highlights

- Global 1-km soil salinity maps reveal 2000–2024 desalinization trends and heterogeneity
- Salinization hotspots in tropical Africa and Asia, high latitudes, and agricultural zones
- Soil evaporation drives >62% of salinity variation; 1-year lag effects dominate zones
- Climate extremes influence salinization areas more than desalinization regions

Wang et al., 2026, One Earth 9, 101658
May 15, 2026
https://doi.org/10.1016/j.oneear.2026.101658

CellPress

One Earth

CellPress

Article

Mapping 25 years of global soil salinity: Hydrothermal conditions drive widespread desalinization amid regional salinization hotspots

Nan Wang,[1,2] Dietian Yu,[1] Songchao Chen,[1] Jingyi Huang,[3] Ruhollah Taghizadeh-Mehrjardi,[4] Jie Peng,[5] Jean-Pierre Wigneron,[6] Frederic Frappart,[6] Asim Biswas,[7] and Zhou Shi[1,8,9,*]

[1]Zhejiang Key Laboratory of Agricultural Remote Sensing and Information Technology, Zhejiang University, Hangzhou 310058, China
[2]Department of Earth System Science, Ministry of Education Key Laboratory for Earth System Modeling, Institute for Global Change Studies, Tsinghua University, Beijing 100084, China
[3]University of Wisconsin-Madison, Department of Soil and Environmental Sciences, 1525 Observatory Drive, Madison, WI 53706, USA
[4]Department of Geosciences, University of Tübingen, Tübingen, Germany
[5]College of Agriculture, Tarim University, Alar 843300, China
[6]ISPA, Bordeaux Sciences Agro, INRAE, 33140 Villenave d'Ornon, France
[7]School of Environmental Sciences, University of Guelph, Guelph, ON N1G 2W1, Canada
[8]Key Laboratory of Spectroscopy Sensing, Ministry of Agriculture, Hangzhou 310058, China
[9]Lead contact
*Correspondence: shizhou@zju.edu.cn
https://doi.org/10.1016/j.oneear.2026.101658

SCIENCE FOR SOCIETY Soil salinization degrades agricultural lands and reduces crop yields, threatening global food security. However, recent global patterns and drivers of soil salinity remain poorly understood. This research provides the first digital soil maps of global soil salinity changes over the past 25 years. The findings reveal that while many regions are becoming less saline, concerning salinization hotspots are emerging in tropical Africa and Asia, precisely where the world grows its rice and wheat. The study identifies soil evaporation, influenced by climate change, as the primary driver of these changes. The long-term ambition is to translate these scientific insights into practical tools for farmers, policymakers, and land managers. This research identifies priority regions for intervention, including Australia, southern Africa, western United States, the Middle East, and Central Asia. These findings enable targeted allocation of resources for soil remediation and sustainable agricultural practices. The work opens avenues for transdisciplinary collaboration with agronomists, hydrologists, and local communities to develop climate-informed soil management strategies. Ultimately, this research provides the scientific foundation for policy decisions and on-the-ground interventions, supporting efforts to achieve food security and sustainable development goals in a changing climate.

SUMMARY

Climate change is influencing soil salinization and threatening global food security, yet recent global trends in soil salinization and its climate drivers remain unclear. Here, we present 1-km-resolution global soil salinity maps from 2000 to 2024 using machine learning and remote sensing, climate, and geographical data. Results reveal a significant global desalinization trend (Theil-Sen slope -0.019 ± 0.008 dS m^{-1}) with spatial variability, with concerning salinization hotspots emerging in some major agricultural zones. Through random forest and SHAP analysis, we identified soil evaporation as the predominant driver of salinity variations (>62% influence), with 1-year lagged effects being the most significant temporal pattern (>49%). Extreme climate events exerted stronger influence in salinization areas (21%) than desalinization regions (17.7%). This study fills critical gaps in understanding recent salinization dynamics, identifying Australia, southern Africa, western United States, the Middle East, and northern Central Asia as priority intervention regions for targeted, climate-informed soil management strategies.

Please cite this article in press as: Wang et al., Mapping 25 years of global soil salinity: Hydrothermal conditions drive widespread desalinization amid regional salinization hotspots, One Earth (2026), https://doi.org/10.1016/j.oneear.2026.101658

INTRODUCTION

Soil salinization is a major soil degradation issue affecting hundreds of countries around the world.[1,2] More than 1 billion hectares of land and its productivity are affected by salinization, resulting in a 50% reduction in global food production so far in the 21st century, resulting in annual global agricultural losses of approximately US$1.27–2.73 billion.[3] Cultivated land affected by soluble salts is mainly distributed in China, India, Pakistan, Iran, Australia, and the United States.[3] Climate and topography are the main driving factors that determine the accumulation and dissolution of soluble salts in soils.[4] With processes such as evaporation, water vapor transport, condensation, infiltration, and runoff in the water cycle, the accumulation of salt in the soil is restricted by moisture transport.[5] Extreme soil temperature, limited precipitation, and heightened evapotranspiration significantly amplify water movement within the soil, aggravating soil salinization.[6] Typically, soil salinization tends to intensify with the combined effects of sea-level intrusion, high evapotranspiration, precipitation decrease, high soil temperature, and improper irrigation management. The overarching global trends in soil salinization across time significantly influence soil sustainability and arable capacity.[7,8]

In the long term, climate change (e.g., global warming, drought, and groundwater intrusion) induced soil drying and wetting cycles are major precursors for soil salinization.[9,10] Typically, with the combined effects of sea-level intrusion, high evapotranspiration, precipitation decrease, high soil temperature, and improper irrigation management, soil salinization tends to intensify.[11,12] Soil salinization maps are essential for understanding trends and environmental responses. To investigate saline soils, the World Reference Base (WRB) for Soil Resources made a commendable effort by classifying the distribution of saline soils at 250-m resolution. However, the resulting classification map may benefit from additional detail to better support specific land management needs. Similarly, the World Soil Information Service (WoSIS) of International Soil Reference and Information Centre documents lack temporal resolution, since the salt soil surveys in different years around the world are not available. Global soil salinity surveys and mapping (e.g., WRB) are time consuming and labor intensive, and only a rough approximation of the extent or qualitative content of saline soils can be obtained.

As an alternative to survey-based soil salinity maps, remote sensing methods can enable high-precision monitoring of soil salinization by compiling field observations. Recent studies have employed remote-sensing-based methods to estimate soil salinization from regional to global scales with its response to climates and moisture change. Ivushkin et al.[9] classified global soil salinization in 1986, 2000, 2002, 2005, 2009, and 2016 (testing accuracy of 67%–70%) by integrating SoilGrids data, Landsat-5/-8 images, and the WoSIS database (snapshot. 2016), providing the possibility for the global quantitative estimation of multiyear soil salinization data. Analyzing the correlation between soil salinization changes and influencing factors at the regional scale, Kawser et al.[13] reported a significant reduction of about 22 dS m^{-1} in soil salinity from 1996 to 2019 in coastal areas of Bangladesh driven by precipitation, tides, and temperature. Bannari and Al-Ali[14] observed an increased trend of salinity on the Indramayu coast correlated with the increasing temperature and decreasing precipitation between 1987 and 2017. Corwin[15] concluded that climate change mainly determines salinity changes in United States farmland by affecting soil moisture, while the impact of climate change on soil salinization varied across space and time at different scales. The limited availability of soil observations poses a challenge to producing comprehensive global multiyear salinity maps. Consequently, the global trend of soil salinization in response to climate and environmental changes remains unclear.

Here, we address the lack of long-term global soil salinization time-series data and its unclear response to climate conditions. We first compiled and reconstructed a multiyear global dataset of measured soil salinity samples from multiple sources, creating a ground-truth reference with extensive spatial and temporal coverage. Using Google Earth Engine (GEE), we then generated annual 1-km-resolution global soil salinity maps from 2000 to 2024 by integrating remote sensing, climate, and geographical data with random forest (RF) regression models trained on this sample dataset. Based on these maps, we applied Theil-Sen (TS) trend analysis to quantify the magnitude and significance of spatiotemporal salinization trends across different climate regions, enabling systematic assessment of global desalinization patterns and localized salinization hotspots. We further employed Shapley additive explanations (SHAP) analysis within the RF framework to identify the primary drivers of soil salinity variations, quantify their relative contributions, and determine the time-lag effects of key hydrological and thermal factors on salt accumulation and dissolution processes. This systematic assessment fills critical gaps in understanding global salinization dynamics and their climatic controls, providing a scientific foundation for developing targeted, climate-informed soil management strategies worldwide.

RESULTS

Global soil salinization trends

To quantify global-scale spatiotemporal patterns of soil salinity change over the past 25 years, we first analyzed soil salinity trends from 2000 to 2024 using the Mann-Kendall (MK) significance test and TS trend analysis at 1-km resolution. After the significance test, the overall significant trend of TS slopes ranged from −1.397 to 0.919, with an average slope of -0.019 ± 0.008 dS m^{-1}, indicating an overall desalinization trend. Soils in hyper-arid, arid, semi-arid, dry sub-humid, and humid regions exhibited a significant desalinization trend, with average slopes below −0.089 dS m^{-1}. Despite widespread desalinization, notable salinization trends were detected in tropical regions of Africa and Asia (approximately 0–25° N). Soil salinity changes showed strong spatial heterogeneity. Increased salinization was also observed in high-latitude regions, such as northern North America and northern Russia (Figure 1B). These patterns reflect the coexistence of global desalinization with localized salinization risks, particularly in tropical zones, Central Africa, and India. Many major agricultural regions are producers of rice and wheat (including tropical areas in Southeast Asia, Latin America, and parts of Africa and India) but showed a soil salinization trend over the past 25 years. Central Africa, identified as a priority for future agricultural development, also showed

Please cite this article in press as: Wang et al., Mapping 25 years of global soil salinity: Hydrothermal conditions drive widespread desalinization amid regional salinization hotspots, One Earth (2026), https://doi.org/10.1016/j.oneear.2026.101658

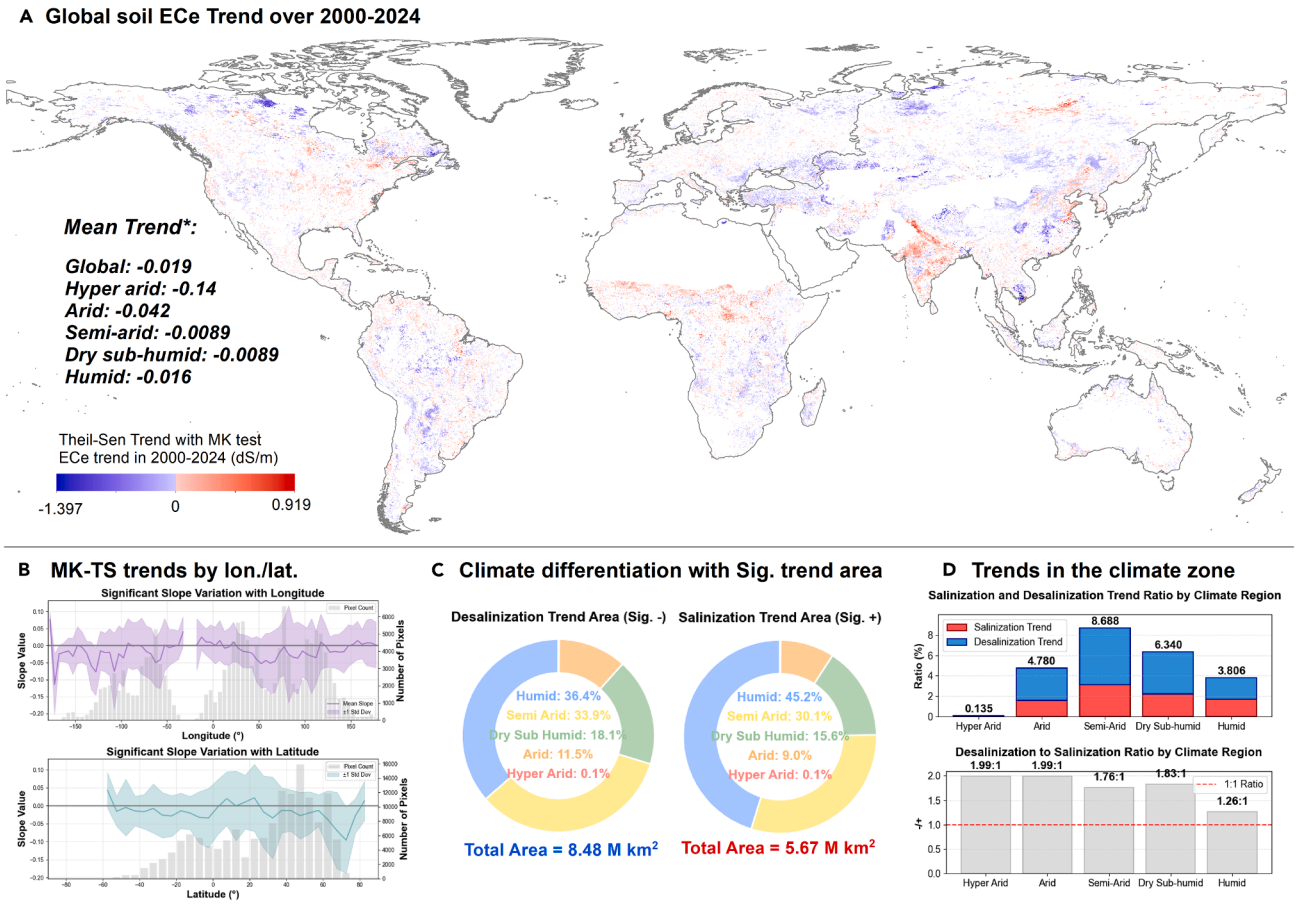

Figure 1. Global soil salinization significance trend map

(A) Mask map of soil salinization trend at 95% confidence interval showing the distribution of areas with significant changes in salinity from 2000 to 2024 globally but masked by deserts and perennially flooded areas.

(B) Average of the significant MK-TS slope by longitude and latitude. (C) The area of soil in salinization trend and desalinization trend, summarized by hyper-arid, arid, semi-arid, dry sub-humid, and humid regions.

(D) The proportion of salinization and desalinization area, with their ratio, in hyper-arid, arid, semi-arid, dry sub-humid, and humid regions.

increasing salinity. These trends suggest that future crop production in these regions may be constrained by soil salinity.

Globally, the area with significantly increased soil salinization reached 5.67 million km^2, while the area with desalinization was approximately 8.48 million km^2. Across climate regions, the order of affected areas is as follows: humid region > semi-arid region > dry sub-humid region > arid region > hyper-arid region (Figure 1C). This distribution is influenced by the inherently uneven global distribution of climate zones. However, as shown in Figure 1D, the semi-arid region had the highest proportion of area with changed soil salinization (8.69%), followed by the dry sub-humid region (6.34%) and the arid region (4.78%). In these regions, arid climatic conditions and frequent human activities contribute to more widespread changes in soil salinity. Furthermore, soil salinization trends in humid regions may be gradually intensifying (ratio 1.26:1, Figure 1D) than drier regions, particularly in northern Russia, coastal North America, and coastal South America, where increased salinization has been observed. These anomalous salinization phenomena highlight the need to address emerging risk patterns associated with climate change. Together, these results reveal the coexistence of global desalinization with localized salinization risks, establishing the spatial basis for subsequent analysis of climatic drivers and priority intervention regions.

Global spatial and temporal patterns of soil salinity

To further characterize the detailed spatiotemporal evolution of soil salinity over the study period, we analyzed annual global topsoil electrical conductivity measured in saturation solution (EC_e) values from 2000 to 2024 at 1-km resolution, estimated using climate-delineated RF models trained on multitemporal soil salinity datasets (methods and supplemental information). Figure 2 shows trends in average EC_e values at the global scale and across the five climate regions from 2000 to 2024. In addition, the phased salinization trend was calculated using 5-year time windows (2000–2004, 2005–2009, 2010–2014, 2015–2019, and 2020–2024). Global salinization showed a significant trend of desalinization with a slope of −0.0056. The results of linear slope with significance test globe wide (Figure 2) are consistent with the TS trend estimates (Figure 1). Overall, soils

Please cite this article in press as: Wang et al., Mapping 25 years of global soil salinity: Hydrothermal conditions drive widespread desalinization amid regional salinization hotspots, One Earth (2026), https://doi.org/10.1016/j.oneear.2026.101658

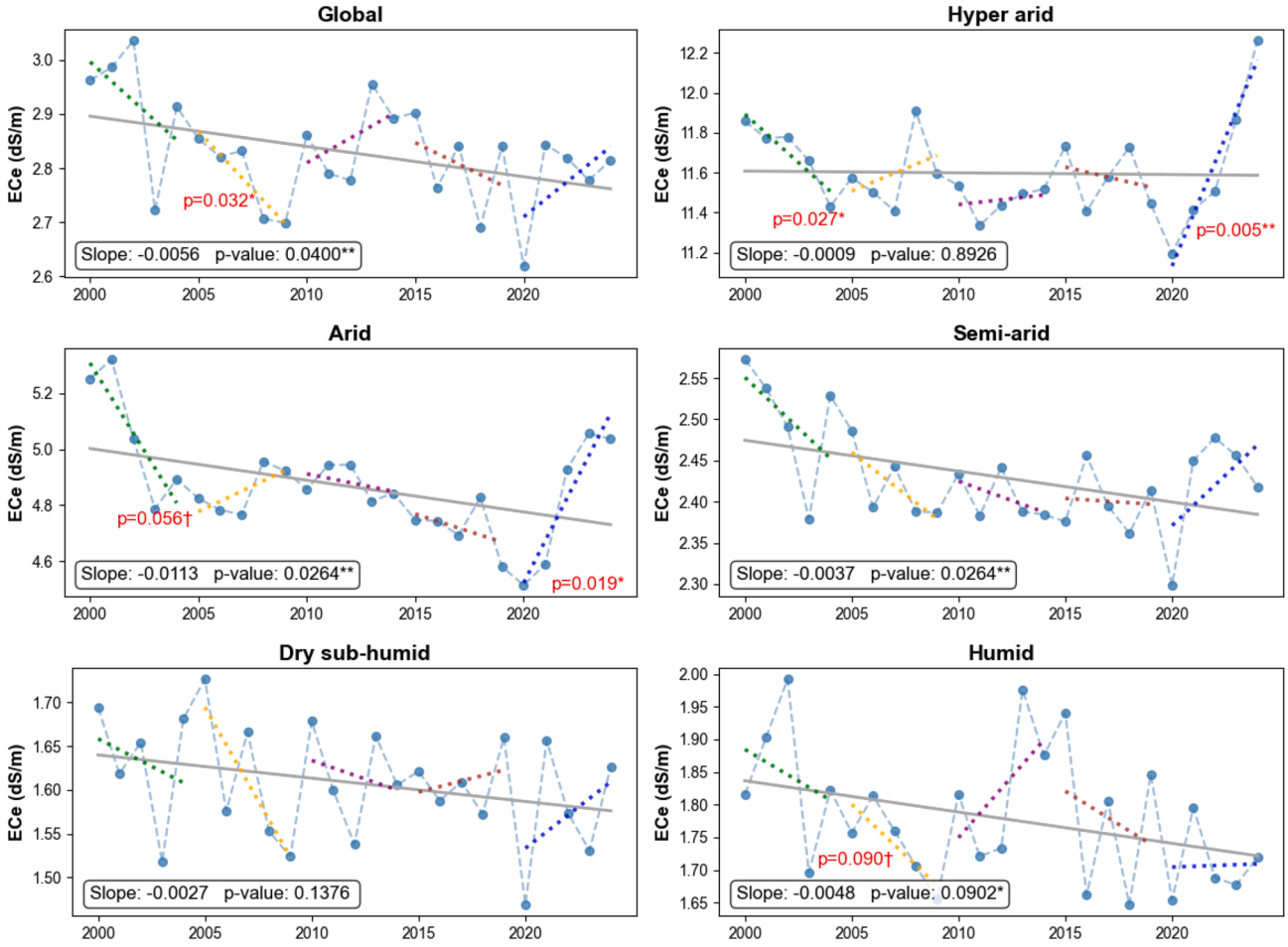

Figure 2. Soil salinization changes of slope from 2000 to 2024

The line chart shows the linear fit of annual average changes in salinity over the past 25 years globally and in hyper-arid, arid, semi-arid, dry sub-humid, and humid regions. Each figure shows salinization change slope at every 5 years (2000–2004, 2005–2009, 2010–2014, 2015–2019, and 2020–2024).

in arid, semi-arid, and humid regions showed a significant decreasing trend in salinity over the past 25 years. In hyper-arid, arid, and semi-arid regions, soil salinization generally decreased during 2000–2020, but an increasing trend has been observed since 2020. However, based on the average values, salinity levels have declined after a high value in 2021. From 2000 to 2024, global soil salinity also shows a fluctuating decline, consistent with the findings of Thorslund et al.,[16] who found that in the Murray-Darling River basin (southeastern Australia, flowing through a semi-arid region) and the Danube River basin (Europe), the salinity flowing through semi-arid, dry, semi-humid and humid regions was mainly decreasing during 1980–2020.

Figure 3 shows the difference between the estimated soil EC_e values in 2024 and 2000, categorized into areas where soil salinity deteriorated from non-saline ($\leq$2 dS m^{-1}) to saline (>2 dS m^{-1}), shown in brown, and areas where salinity improved from saline to non-saline, shown in blue. Figure 3 indicates that the area of soil changing from saline soil to non-saline soil (7.63 M km^2) is higher than the area of deterioration (6.17 M km^2). Soil in the northern part of the Central Asian continent is transformed into saline soil, and the trend here is the highest. In the desert margins of the hyper-arid region, such as the southern part of the Sahara Desert in Africa, the eastern part of the Australian desert, and the eastern part of the Thar Desert, there is greater distribution of saline soils. The arid climate and the process of desertification may have led to the transformation of healthy soils into saline soils. Soil improvement is apparent around waters or seashores of Australia, eastern China, eastern North America, and South America. This may be related to water conservancy projects and soil improvement projects in near-water areas and coastal saline soils. In high-latitude regions, the salinization of saline soil is more frequent, which may be related to heavy precipitation and a humid climate. The transition of non-saline to saline soil occurs in eastern North America, eastern South America, southern Africa, central Africa, India, eastern Australia, eastern China, northern Southeast Asia, and high-latitude regions. We found that although there is a desalinization MK-TS trend in southern Africa, southern South America, and northern Southeast Asia, the soil in these regions is still dominated by the transition of saline soil in absolute terms. This might be due to the soil salt content values in these regions being

Please cite this article in press as: Wang et al., Mapping 25 years of global soil salinity: Hydrothermal conditions drive widespread desalinization amid regional salinization hotspots, One Earth (2026), https://doi.org/10.1016/j.oneear.2026.101658

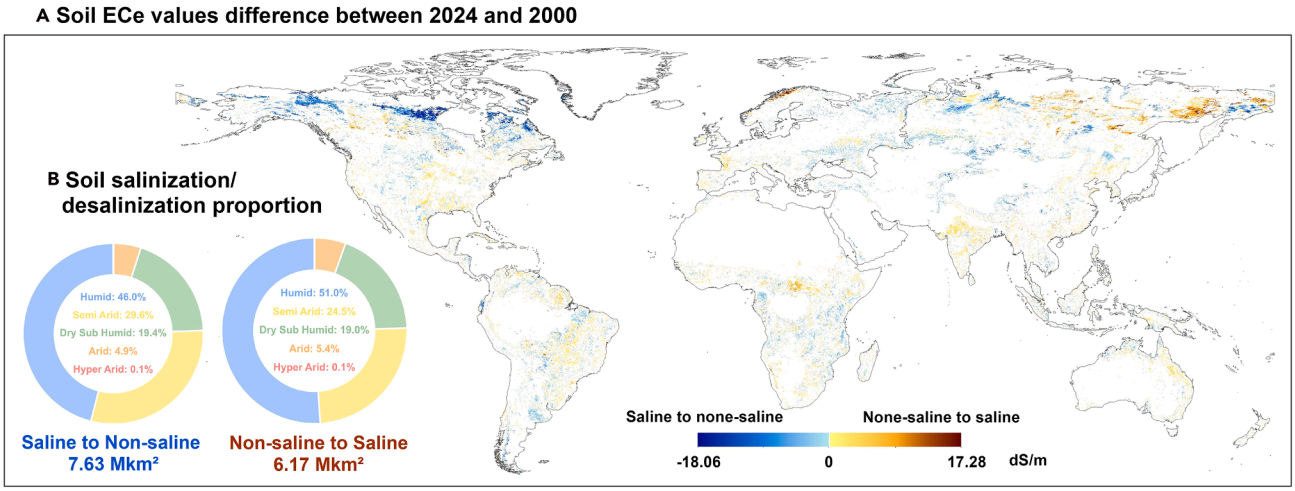

Figure 3. Transition of saline soil and non-saline soils between 2024 and 2000, with convert proportion

(A) From 2000 to 2024, blue indicates the area where the saline soil is transformed into non-saline soil and its transition difference value, while red indicates the area where the non-saline soil is transformed into saline soil and its transition difference value.

(B) The area and proportion of the two types of soil transformation were calculated, respectively, in five climate regions.

inherently high, but the trend calculation only focuses on this tendency. Therefore, the trend and the absolute value of salt content need to be considered comprehensively. Together, these results reveal the complex interplay between gradual trends and abrupt transitions in global soil salinity, providing essential context for identifying regions requiring priority intervention and informing targeted management strategies.

Time-series responses of soil salinity to hydrothermal conditions

To identify the key climatic drivers governing soil salinization dynamics and their temporal mechanisms, we evaluated the impact of six key environmental factors on soil salinization trends (MK-TS slope), including four hydrothermal factors (soil moisture, precipitation, soil temperature, and soil evaporation) and two extreme climate indicators (consecutive dry days and summer days). Our results indicate that soil salinization trends are influenced by climate and moisture content in the soil. Water drives soil salinization through time lags (delays).[17,18] The spatial distribution of the main driving factors is shown in Figures 4A and 4B, while their temporal effects on soil salinization dynamics are presented in Figures 4C and 4D. Through RF regression and SHAP analysis (supplemental information), we found that changes in soil evaporation constituted the dominant factor influencing soil salinity variation across all five climate zones (>62%), followed by summer days. Evaporation played a direct role in capillary-driven salt transport: higher evaporation rates draw saline groundwater to the surface, leaving dissolved salts to accumulate in the root zone.

As climatic humidity increases, extreme temperature and drought factors (consecutive dry days and summer days) exhibit stronger driving effects, particularly in high-latitude regions such as northern North America and northern Europe. This pattern is driven by increased evaporative demand under warmer conditions, which concentrates salts at the surface, while extended dry periods simultaneously reduce leaching efficiency. Changes in soil hydrothermal conditions, especially soil evaporation, play a more significant role in driving desalinization compared to salinization areas. This may be because sustained evaporation reduction allows precipitation to effectively leach salts from the soil profile. In contrast, extreme weather events exert stronger influence in regions experiencing intensified salinization (21%) than in desalinization areas (17.7%), as short-term climate extremes can rapidly trigger salt accumulation through concentrated evaporation pulses.

Results from time-lag effect analysis reveal that the 1-year lag effect was the most dominant temporal factor (>49%) across all five climate zones, followed by original feature changes (without lag). Salt transport through soil profiles and groundwater systems requires considerable time due to low solute velocities and complex soil-water interaction. Therefore, soil salinity showed hysteresis to environmental changes.[19] The influence of time-lag effects increases with regional aridity, as drier conditions typically feature thicker unsaturated zones and longer solute residence times. Accordingly, soil salinity changes in western South America, Central Africa, India, western Asia, and eastern Asia are more substantially influenced by these temporal effects. Furthermore, the time effect plays a stronger role in areas undergoing desalinization (84.5%) compared to those with increasing salinity (81.8%), possibly because salt leaching represents a more gradual process compared to the relatively rapid salt accumulation during evaporation-dominated periods. Together, these findings establish evaporation-driven processes as the primary control on global salinization dynamics, with time-lagged responses and extreme events modulating regional patterns, providing a mechanistic basis for predicting future salinity changes under evolving climatic conditions.

DISCUSSION

According to the process of salt migration and accumulation in soil, the change of salt content in soil is determined by vegetation,

Please cite this article in press as: Wang et al., Mapping 25 years of global soil salinity: Hydrothermal conditions drive widespread desalinization amid regional salinization hotspots, One Earth (2026), https://doi.org/10.1016/j.oneear.2026.101658

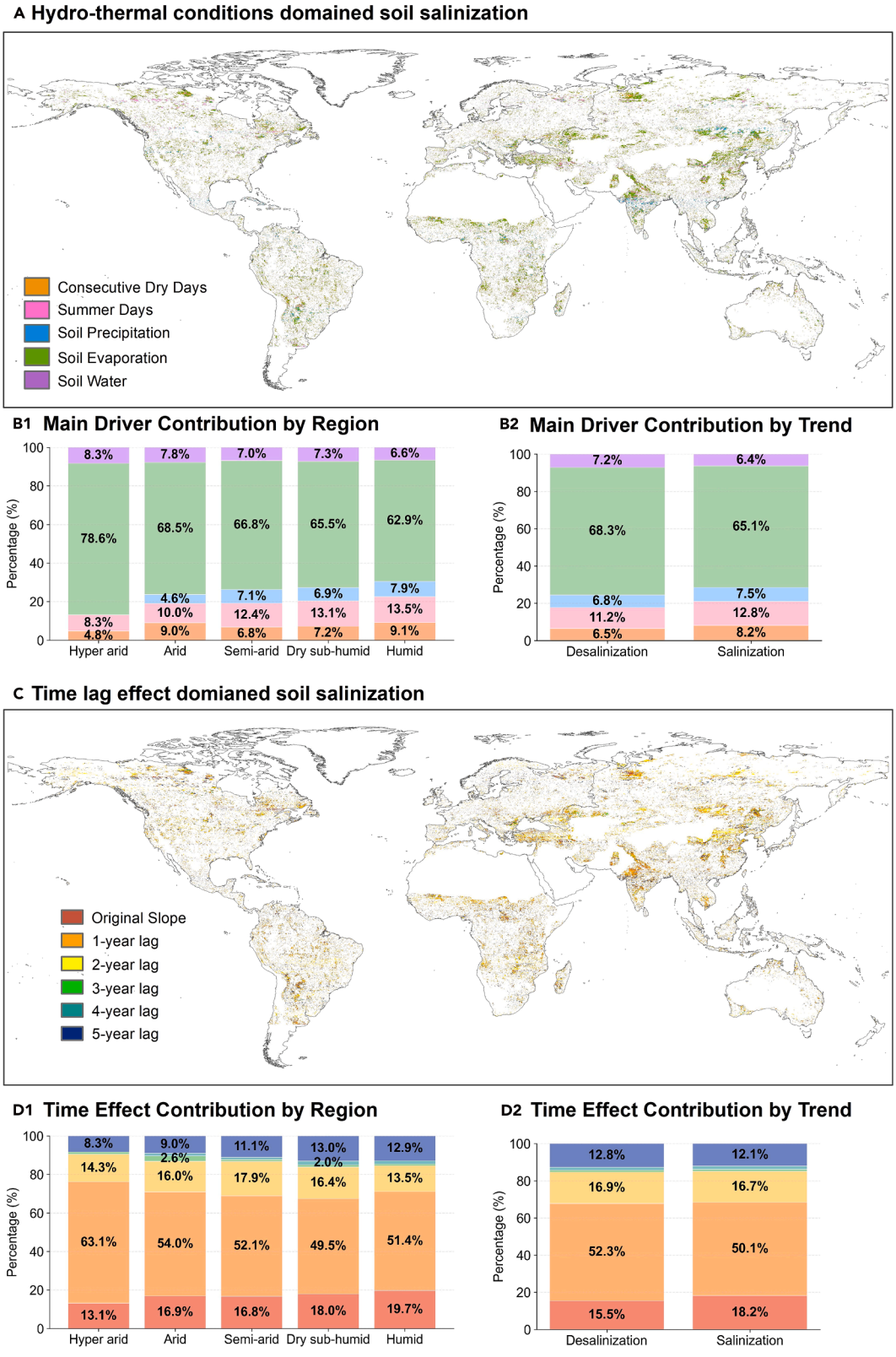

(legend on next page)

Please cite this article in press as: Wang et al., Mapping 25 years of global soil salinity: Hydrothermal conditions drive widespread desalinization amid regional salinization hotspots, One Earth (2026), https://doi.org/10.1016/j.oneear.2026.101658

soil moisture, climate, and topography. The scarcity of precipitation and intense soil evapotranspiration caused by arid climatic conditions lead to the rise of soil water, and the salt in the parent material cannot be discharged and accumulates in the soil, which is the main driving force of soil salinization in hyper-arid, arid, and semi-arid regions. In dry sub-humid and humid regions, the seasonal freeze-thaw process of soil in moist high latitudes leads to the accumulation of stagnant salt. Under the influence of leaching and topography, accumulated salt moves from high places to low-lying places with poor drainage, resulting in the aggravation of soil salinization. On the seashore, the soil in the coastal area is soaked by the soluble salt in the sea water to form salinization by the erosion of sea water. Various drivers jointly contribute to the changes in soil salinity, but in remote sensing estimation, variables showed different sensitivity. Notwithstanding the regional specificities, the climate, groundwater depth, vegetation, and soil condition demonstrated universal importance across all climates in the models.[20] These factors collectively represent fundamental components of the salt balance equation, including the control of salt input, transport, and concentration. Evaporation and precipitation define the regional water balance, determining whether salts are leached or concentrated.[5] Groundwater depth directly regulates salt sources and transport pathways, while soil conditions control capillary action and drainage capacity.[21] Vegetation serves as a bio-indicator integrating overall soil health and vegetation response to salinity stress.[22] Furthermore, vegetation indices exhibited stronger explanatory power in drier regions (hyper-arid and arid), where plants function as sensitive indicators of minimal changes in soil salinity and water availability. Conversely, climate variables (particularly evaporation and precipitation) dominated in more humid regions (dry sub-humid and humid), where energy and water balances primarily modulate salt accumulation through the interplay between leaching events and evaporative concentration. These findings systematically reveal both the divergent mechanisms and common principles governing soil salinization across climatic gradients (supplemental information). In the modeling process, the unevenly distributed soil samples across different regions may cause uncertainty. There is a high concentration of data from North America and Europe, while Asia and South America are under-represented. Additionally, the hyper-arid region itself has a relatively small land area globally and contains large deserts (e.g., the Sahara Desert). Therefore, the area of masked soil is small, and soil sample points are very limited in the dataset. This spatial and categorical imbalance introduces uncertainty in model predictions. In the modeling, imbalanced training data caused overfit in densely sampled regions and performed poorly in areas with few samples. As a result, soil salinity may be overestimated in data-rich regions (e.g., North America and Europe) while being underestimated in areas with sparse training data (e.g., Central Asia and South America). These local biases tend to counterbalance each other at the global scale, thereby minimizing the overall impact on the model's accuracy.[9]

Combining the dynamic trend of soil salinization changes (Figure 1) and the absolute values of changes in saline soil types (Figure 2), we found regions where the trend of soil salinization is intensifying (such as India, northeastern China, Central Africa, and central North America). In addition, we have also observed that in some areas, although the soil shows a dynamic trend of desalinization, the absolute value still indicates an increase in saline soil. These regions include southern Africa, southern North America, eastern South America, Europe, and eastern Australia, among others. This might be due to the fact that saline soil is widely distributed in these areas, but the trend is showing a dynamic improvement. In the map of TS-MK slope of soil salinization change, the areas with increasing soil salinization trends were in accordance with the results reported in previous studies,[23] which observed soil salinization over years in hyper-arid regions such as Uzbekistan and Xinjiang (China).[6,24] High temperatures, sparse precipitation, and strong soil evapotranspiration caused salt accumulation on the topsoil in arid and semi-arid climates.[25] Bhuyan et al.[26] reported an increasing trend of soil salinization in Bangladesh between 2020 and 2021, which is similar to the average soil EC_e values in the arid, semi-arid, and humid regions of Bangladesh, with an increased trend over 2 years (Figure 2). Frequent drought events and seawater intrusion caused soil salinization in coastal soils (e.g., Australia, eastern China, and southern India).[10,15,27] Salt moved and accumulated strongly in deserts in the hyper-arid region, showing strong temporal variability and salinization trend over years, especially in the southern Sahara Desert, southwest of Thar Desert, and southwest of the desert region in Australia (Figure 2). From 2000 to 2010, soil salinity in hyper-arid regions decreased and then increased, while that in arid regions increased and then decreased. Among these data, soil salinity in hyper-arid regions shows a high value in 2008, which was largely influenced by the El Niño southern oscillation.[28]

Precipitation and groundwater in arid areas show a more sensitive detection of soil salinization, mostly groundwater, as the surface water and soil moisture components are negligible in these areas. Eswar et al.[12] found an aggravation of soil salinization in arid and semi-arid regions due to climate change and overexploitation of water resources for agricultural irrigation. This proves that the water in climate and soil is the key driver that dominates the changes in soil salinity in drier regions. Human-induced water redistribution can accelerate soil salinization processes in arid climate conditions, overdrawing groundwater extractions, while unmanaged agricultural fertilization results in the reduction and depletion of groundwater levels.[29,30] Soluble salts migrated to the topsoil along with upflowing capillary water

Figure 4. The dominant hydrothermal conditions and the main time effect of soil salinization trend, with proportion calculated in five climate regions

(A) The key drivers of soil salinity change, consisting of consecutive dry days, summer days, soil precipitation, soil evaporation, and soil water.

(B) The percentage of the drivers by region (hyper-arid, arid, semi-arid, dry sub-humid, and humid) and trend types (desalinization and salinization). The color of the column corresponds to the hydrothermal conditions in (A).

(C) The key time effect of soil salinity change, including the original slope and time lag.

(D) The percentage of the key time effect by region (hyper-arid, arid, semi-arid, dry sub-humid, and humid) and trend types (desalinization and salinization). The color of the column corresponds to the time-effect conditions in (C).

Please cite this article in press as: Wang et al., Mapping 25 years of global soil salinity: Hydrothermal conditions drive widespread desalinization amid regional salinization hotspots, One Earth (2026), https://doi.org/10.1016/j.oneear.2026.101658

due to the shallowing groundwater, which aggravates soil salinization.[31] For example, previous studies reported that soil salinization increased due to the decline and degradation of groundwater in the UAE,[22] western desert of Egypt,[32] and Tadla plain.[32] Decline in groundwater exacerbated salinization in arid and semi-arid regions, as has been reported in southern Greece for instance,[33] while insignificantly affecting salinity changes in other climates. Figure 1 shows that in areas with increased soil water and decreased soil evaporation in Mongolia, soils showed a significant desalinization trend (Figure S4). In general, soil salinization causes soil productivity to decrease, inhibiting the growth of vegetation and crops. Similarily to results by Alber et al.,[34] the dry climate does not explain the change in salt marshes in the eastern and gulf coasts of the United States. Figure 1 shows a desalinization MK trend in the eastern United States and a salinization MK trend in the western United States. However, the soil evaporation shows an increased slope in the west and a decreased slope in east (Figures S3 and S4). Similarly to results by Alber et al., the east coast of the United States was in a wetter region, but the soil showed a trend toward both salinization and desalinization. Meanwhile, summer days play a certain dominant role in the eastern United States, which simultaneously proves that arid climate may not be able to fully explain the changes in soil salinity (Figure 4), and climate change may exacerbate soil salinization through more frequent extreme drought events.[10,27,35] However, our study assessed the drought trend over the past two decades, and the extreme climate indicators used are also long-term trends, so it may not be possible to clarify the drivers of individual drought events regarding soil salinization. The frequency and change of drought events and the response to soil salinization need further research.[35]

According to the drought legacy effects, the legacies of previous drought are alterations in ecosystem structure and function that persist after the drought event itself has ended, which predominantly influence ecosystem responses to subsequent stress over a period of 1–2 years.[36,37] Müller's research summarized the investigation of the duration after drought based on previous papers. The results show that the research span of the degradation of soil and ecology caused by the year post drought ranges from 0 to 10 years, mostly from 0 to 5 years, and mainly concentrated in 0–3 years.[37] These legacy effects can include reduced carbon reserves, altered microbial communities, and shifts in species composition, which all have a direct bearing on the processes our study investigates. Furthermore, Han et al.[37] proved the hydroclimatic impacts on surface processes. Han's research has shown that while sub-surface groundwater changes can occur over longer seasonal to inter-annual cycles, the most dynamic and measurable responses in surface conditions are often captured at an inter-annual scale. For instance, research on playa surface salinity demonstrates that topsoil salinity responds rapidly to individual hydrological events, while the integrated effect of groundwater dynamics, which drives longer-term salinization trends, is effectively captured at an annual scale rather than a decadal one.[37] We have to admit that few studies have directly reported the inter-annual effects of soil salinization. Therefore, we have chosen drought events closely related to soil salinization for analogical research.

Soil evaporation based on the time effect drives changes in soil salinization. Soil evaporation in the previous year can drive salt accumulation in the following year through multiple mechanisms.[38] First, the lag in the water-salt balance is manifested as high evaporation leading to a reduction in soil moisture and salt surface accumulation, while the leaching effect of precipitation or irrigation requires time to effectively reduce the salt concentration. Under this condition, the salt remains in the soil and affects the degree of salinization in the following year.[39] Second, the high evaporation in dry years will reduce the initial soil moisture content of the following year, thereby intensifying salt accumulation.[39] Meanwhile, the seasonal evaporation-precipitation cycle promotes the redistribution of salts in the soil profile.[36,37] Finally, the vegetation feedback mechanism shows that high evaporation will reduce vegetation coverage, weaken biological drainage, and make the soil more prone to salt accumulation in the following year.[21] This time effect is particularly evident in hyper-arid, arid, and semi-arid regions. Corwin et al.[40] used the HYDRUS model to simulate salt migration and found that there was a lag in water-salt movement, indicating that the water moves faster than salt. In addition, extreme climate events can also affect soil salinization. For instance, an increase in heat waves and the number of summer days (the number of days with a daily maximum temperature above 25°C) will enhance the surface evaporation potential. This leads to an enhancement of soil capillary action, promoting the upward migration of deep salts with water and their accumulation on the surface layer, thereby accelerating the primary salinization process in arid and semi-arid regions. The extension of the number of consecutive drought days (CDD) will intensify soil moisture deficiency and completely block the leaching effect of natural precipitation on surface salts. After a long dry period, even if there is heavy rainfall, it often fails to effectively wash away the salt due to the rapid downpour and limited infiltration. On the contrary, the rapid evaporation after rain will cause the dissolved salts to quickly re-accumulate on the soil surface, triggering more severe secondary salinization. Therefore, under the background of prolonged CDD, the salt leaching effect of heavy rainfall events decreases and the salt surface accumulation intensifies. Rengasamy[41] pointed out that as the frequency and intensity of heat waves increase, the demand for atmospheric evaporation rises, which directly intensifies soil capillary action, lifting saline groundwater to the root zone and causing salt accumulation in the surface soil, which is the main driving factor of primary salinization in arid areas. Shukla et al.[42] pointed out that climate change has led to prolonged drought periods and a decline in soil moisture content. Moreover, extreme rainfall events are more likely to form runoff on land after drought. The decline in soil water infiltration capacity will affect the leaching of nutrients and the transport of salts. These extreme climate factors jointly increase the inter-annual variability and cumulative risk of surface soil salinity by altering the water and salt balance of the region.

Human activities and socio-economic factors are important factors driving these environmental factors and salt distribution. International and regional soil management policies influence salt distribution. The effects of human activities such as excessive mining, agriculture, groundwater pollution, urbanization, and extreme weather have led to lifting groundwater levels and worsening soil salinization. Abandoned mines and coal gangue pollute soil water and groundwater, leading to the rise in groundwater level and increased salinity. Unreasonable agricultural

Please cite this article in press as: Wang et al., Mapping 25 years of global soil salinity: Hydrothermal conditions drive widespread desalinization amid regional salinization hotspots, One Earth (2026), https://doi.org/10.1016/j.oneear.2026.101658

irrigation and excessive fertilization and grazing cause soil compaction and waterlogging, blocking soil drainage and increasing soluble salt recharge, which aggravates soil salinization. Urbanization has led to reduced vegetation cover and extreme rainfall events, which have intensified soil leaching. In addition, global warming and extreme drought events lead to decreased soil freezing depth, strong evapotranspiration, and violent upward accumulation of salt, resulting in serious secondary salinization. In the arid region of Cholistan Desert in Pakistan, where severe soil salinization is caused by overgrazing, the Pakistan Council of Research in Water Resources proposed a policy in 2006 to manage water for sustainable agriculture.[43,44] In addition, the INIA-Intihuasi (National Institute of Agriculture) in Chile has been working on sustainable agricultural development since 2006.[45] During 2005 and 2016, Israel oversaw the emergency construction of several desalination plants along the Mediterranean coast, promoting sustainable water use and effectively mitigating desertification.[46] Soil improvement in coastal areas can help reduce soil salinization in dry sub-humid and humid areas, which is similar to the trend shown in Figure 2. The Saudi Water Authority released the National Water Strategy in 2018. The theme of the 8th World Soil Day in 2021 is "halt soil salinization, boost soil productivity," and in recent years there has been increased global attention on the impact of saline soil on soil productivity and reducing salinization to replenish arable land. TS salinization trends and the phased salinity trends since 2020 show that soils are tending to be desalinized alongside international and regional attention to saline soils. Since 2020, China has carried out a survey of saline-alkali land and has improved salinized farmland. Especially for farmland in semi-arid areas, the suggestion of salinization policy is confirmed by the trend of average salt content, with a global slope of -0.019 ± 0.008 dS m^{-1} (TS-MK slope, Figure 1) and -0.0056 (linear slope, Figure 2) in 2020–2024. For example, China promotes saline-alkali soil water conservancy in semi-arid areas for soil leaching and salt drainage, promotes the balance of arable land utilization and compensation in coastal saline soil in humid areas, improves reclamation and management of unused saline-alkali land, and has reduced soil salinization since 2020. According to the salinization trend and drivers, land managers and policymakers can use our findings to prevent further salinization. In semi-arid regions (e.g., China), promoting water conservancy projects for soil leaching and sub-surface drainage is critical to remove excess salts. In coastal and humid areas, the focus should be on balancing land use and compensation, improving reclamation techniques, and managing water tables to prevent saltwater intrusion and capillary rise. In arid regions, the priority must be on sustainable water-use policies (e.g., Israel and Saudi Arabia) to prevent secondary salinization caused by high evaporation and unsustainable irrigation.

In the comparison of the Global Map of Salt-affected Soils (GSASmap) of UN Food and Agriculture Organization,[47] the recent observations of this study, and the future salinization risk prediction of Hassani et al.,[48] similar conclusions were reached in the global soil salinization hotspots. Five key risk areas were summarized from different time dimensions: Australia, southern Africa, western/southwestern United States, the Middle East, and northern Central Asia. Specifically, the GSASmap emphasizes Australia (particularly the south and west) as a saline soil distribution area. Our research observed that the soil in eastern Australia is salinizing, with complex salt dynamics, and it is predicted in the future risk map to be a major hotspot for intensified salinization. Regarding South Africa, the GSASmap points out that this region is a concentrated area of saline soil in Africa. Our research confirms that the absolute value of soil salinity is still mainly salinized, and it is also listed as one of the countries with the highest future risk in the future risk map. The GSASmap identifies western/southwestern United States as the main distribution area of saline soil in North America. Our results show the trend of high-latitude salinization in North America, and the future risk map also predicts that salinization in the southwestern United States will intensify. With regard to the Middle East (Arabian Peninsula and Iran), the GSASmap has identified it as the core distribution area of saline soil. Our results reveal a strong trend of salinization, and the future risk map also shows the intensification of salinization in arid areas; Northern Central Asia is marked by the GSASmap as the main area for the distribution of saline soil, and our results indicate that this region is one of the areas with the strongest tendency for soil to transform into saline soil. Although Hassani et al.[48] predicted a decrease in salt content in the region in the future, based on the results of the GSASmap, we can still infer that the salinization in northern Central Asia is intensifying. Based on this conclusion, policymakers need to give priority to the treatment of saline soil and sustainable agricultural management in these regions. In the short term, immediate containment and adaptive measures should be taken in regions where a deteriorating trend is observed, such as Central Asia and eastern Australia. In the long term, water-saving agriculture, salt-tolerant crop breeding, and intelligent monitoring can be laid out in areas with increased risks (such as the southwestern United States and southern Africa) based on climate predictions (especially evapotranspiration and precipitation). Building on the proposed saline soil management framework, region-specific adaptation is crucial. In Central Asia, where irrigation-induced salinization prevails, salt-tolerant crop breeding can be combined with localized phytoremediation. For example, in Uzbekistan and Kazakhstan, cultivating native halophytes (e.g., *Atriplex* spp. and *Kochia scoparia*) alongside salt-resistant sorghum and quinoa improves soil structure and provides fodder and bioenergy, supporting both ecological and livelihood resilience in arid zone.[49,50] This integrated approach links genetic adaptation with agro-ecological rehabilitation to address salinity and socio-economic needs. In regions like southern Ukraine's dry steppes, where seasonal waterlogging and secondary salinization occur, precision land management has been adapted to local hydrology. Laser leveling combined with sub-surface drainage and chemical amendments (e.g., phosphogypsum) reduces surface salt accumulation and enhances water-use efficiency.[49,51] Strategies that combine salt-tolerant crops with tailored water and soil management, designed in response to local agro-climatic and socio-economic conditions, are effective for saline soil remediation.

We focus on a dynamic and lag-explicit temporal perspective on soil salinization and have developed a novel data and modeling framework for global change analysis. The results offer both methodological and practical value for monitoring global soil salinity change. Methodologically, the integrated

Please cite this article in press as: Wang et al., Mapping 25 years of global soil salinity: Hydrothermal conditions drive widespread desalinization amid regional salinization hotspots, One Earth (2026), https://doi.org/10.1016/j.oneear.2026.101658

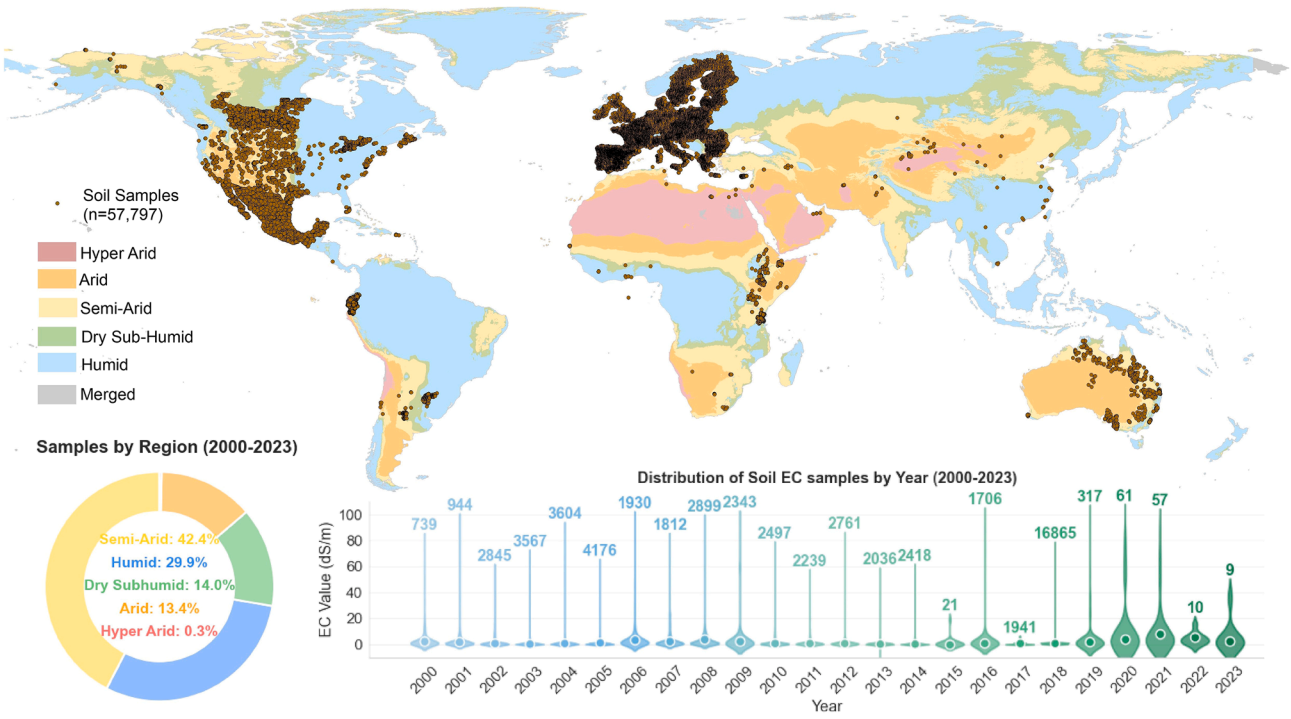

Figure 5. Global distribution of soil datasets for training and testing

Spatial distribution and salt value statistics of soil samples in the five climate regions globally and number of samples with EC_e values for the five climate regions. The total samples are classified into time-series datasets from 2000 to 2024.

framework combines a unified global EC_e dataset with a dynamic model that accounts for lag effects, which provides a reusable approach for analyzing environmental changes over time. In contrast to conventional static mapping, our method captures temporal trends in salinity, helping to identify not only where changes occur but also how environmental drivers influence those changes across years. This approach can also be applied to other slow-onset processes such as desertification or soil carbon change, where time lags and spatial variability pose similar challenges. In practical terms, the annual maps of salinity change and the analysis of lagged effects offer useful information for land management and policy planning. By showing how earlier environmental conditions affect later salinity levels, our results can aid in early detection of soil degradation in sensitive areas. The global EC_e dataset developed in this study may also serve as a reference for validating regional models and guiding future surveys. In addition, the set of predictors and the zoning-based modeling strategy can help improve the design of monitoring systems, especially in regions with limited data. While further testing is needed, this study establishes a practical foundation for more predictive and process-informed assessment of soil salinity worldwide.

METHODS

Climate regions and global soil salinity datasets

According to soil-forming theory,[52] climate,[53] parent material,[54] biota,[55] and relief[56] contribute most to the accumulation and dissolution of soil salt. The impact of floods and tides on soil can be indirectly characterized by groundwater, precipitation, and soil moisture content.[3] Soils in glaciers, permafrost, deserts, and seawater-submerged areas are unsuitable for plant growth or land use, so these areas were not considered in this study. Global desert, tundra, and frost were masked by the Koppen-Geiger system.[57] The global extent of intertidal areas and floods was masked using the Murray Global Intertidal Change Dataset and Global Flood Database from Terra and Aqua MODIS sensors (UQ/murray/Intertidal/v1_1/global_intertidal).[58,59] The aridity index (AI, ~1 km) from the Global Aridity Index and Potential Evapo-Transpiration Climate Database was used to delineate global climate regions to five climate regions: hyper-arid ($AI < 0.03$), arid ($0.03 < AI < 0.2$), semi-arid ($0.2 < AI < 0.5$), dry sub-humid ($0.5 < AI < 0.65$), and humid ($AI > 0.65$) regions (Figure 5).[60]

The global temporal saline soil datasets were assembled from open-source datasets, field investigation, and meta-analyses. Specifically, the soil sample collection strategy encompassed data from the following sources: (1) existing soil datasets that explicitly report sampling time and EC_e; (2) conversion from other forms of soil EC data using empirical formulas (e.g., from $EC_{1:5}$ to EC_e); and (3) meta-analysis. The soil databases utilized include WoSIS datasets, Canada Detailed Soil Survey (DSS), Land Use/Cover Area Frame Statistical Survey (LUCAS), Soil Information System of Latin America and the Caribbean (SISLAC), Africa Soil Profiles Database, and National Cooperative Soil Survey (NCSS) (supplemental information). The meta-analysis was used to extract samples from previous papers in Iran, Vietnam, Pakistan, Tunisia, China,

Please cite this article in press as: Wang et al., Mapping 25 years of global soil salinity: Hydrothermal conditions drive widespread desalinization amid regional salinization hotspots, One Earth (2026), https://doi.org/10.1016/j.oneear.2026.101658

Table 1. Descriptive statistics of datasets for soil salinity estimation in five climate regions

Climate region	Dataset	Number	Maximum	Minimum	Mean	Standard deviation	Skew
Hyper-arid	training	116	88.03	0.0	6.07	13.84	4.03
	testing	58	60.80	0.0	5.42	10.67	3.82
Arid	training	5,117	98.08	0.0	3.55	9.70	5.67
	testing	2,627	97.30	0.0	3.99	10.96	5.50
Semi-arid	training	17,034	97.50	0.0	1.83	4.13	9.32
	testing	7,471	81.20	0.0	1.83	4.34	7.70
Dry sub-humid	training	5,760	96.00	0.0	1.14	4.41	12.62
	testing	2,331	75.00	0.0	1.16	4.18	10.27
Humid	training	12,263	96.00	0.0	1.29	6.27	10.55
	testing	5,018	96.00	0.0	1.37	6.66	9.73

Egypt, Turkey, United States, Kazakhstan, Jordan, Spain, and Mexico. A total of 57,797 topsoil salinity samples remained[61,62] (Figure 5). Soil EC values were measured from the water-saturated soil paste to represent soil salinization. All the data were used to train and test the time-series regression model according to the time series 2000–2024. The number of sample points and salinization level in each year are shown in Figure 5. The soil salinity samples of five climate regions were randomly divided into training and independent testing sets by a ratio of 7:3, as shown in Table 1.

Covariate datasets for modeling

Driven by the Earth's water cycle, salt accumulation in soil is determined by climate, water, soil conditions, vegetation, and topography (Figure 6). Climatic factors determine soil salinization by affecting regional drought, precipitation, and soil evapotranspiration. Influenced by climate conditions, the migration of soluble salts changes with soil moisture, groundwater level, and the topography patterns. Vegetation coverage, soil physical, and soil chemical properties observed through remote sensing can be indirectly used to monitor soil salinization. The SCORPAN model provides a robust framework for understanding the spatial factors (soil, climate, organisms, relief, parent material, age, and spatial position) that influence soil properties, including salinity.[20] The salinization process is essentially the accumulation of soluble salts via capillary rise and water movement, influenced by the hydrological cycle. The specific roles of the covariates are as follows. First, climate provides the dominant energy and water inputs that drive the salt balance.[63] The interplay between precipitation and evapotranspiration is the most important. Low precipitation fails to leach salts from the root zone, while high evapotranspiration creates a strong upward hydraulic gradient, pulling saline groundwater toward the surface through capillary action. Second, topography dictates the gravitational movement of water.[21] It concentrates both surface water (runoff) and sub-surface flow in low-lying, poorly drained depressions. These areas become chemical sinks where salts accumulate after being transported from higher elevations. It thus determines the spatial distribution of soil moisture and influences groundwater table depth. Third, soil moisture is the medium in which salts are dissolved and transported, and the flow influences the salt distribution. The upward flow (capillary rise) leads to salt accumulation, while downward flow (leaching) leads to salt removal. It is the direct manifestation of climate forcing and topographic control, and its movement is governed by soil properties.[64] Fourth, soil properties, especially texture and structure, regulate capillary rise and hydraulic conductivity.[65] Fine-textured soils (clay) have strong capillary action but poor drainage, facilitating salt accumulation. Coarse-textured soils (sand) have weak capillary rise but good drainage. Fifth, vegetation changes the water balance through transpiration, which can lower the water table and reduce evaporation, thus interrupting the capillary salt transport.[32] Also, this process is coupled with strong negative feedback whereby increasing soil salinity creates osmotic stress and toxicity, which inhibits plant growth, providing a key indicator for monitoring salinization.

Based on this theory, we conducted a comprehensive review of methodologies and covariate selections employed by leading research groups worldwide, presented in Table 2 (for the references cited therein, supplemental information). Table 2 emphasizes the importance of using an extensive set of covariates to accurately detect and quantify soil salinity. Long-term monitoring studies conducted in countries such as the United States, Portugal, Iran, and China have consistently highlighted the simultaneous observation of factors such as moisture, topography, and vegetation alongside salinity measurements. These international efforts further validate the selection of soil properties, vegetation, soil moisture, climate, and topography as key variables, confirming that they are not only theoretically grounded in physical processes but also empirically supported for monitoring saline soils. Within this spatially explicit framework, we explicitly incorporated a temporal dimension, introducing time as a constraint on the action of these environmental covariates. This enhancement allows the equation to model not just the spatial state but also the temporal change in salinity. According to the process of soil salinization and based on remote sensing data, the soil salinization change formula was constructed as

$$C(Salinity) = f(C, W, S, T, V)^{L} + e, \qquad \text{(Equation 1)}$$

where *Salinity* is soil salinization change, C is climate conditions, W is water, S is soil conditions, T is topography, V is vegetation, L represents time-lag effects, and e is error.

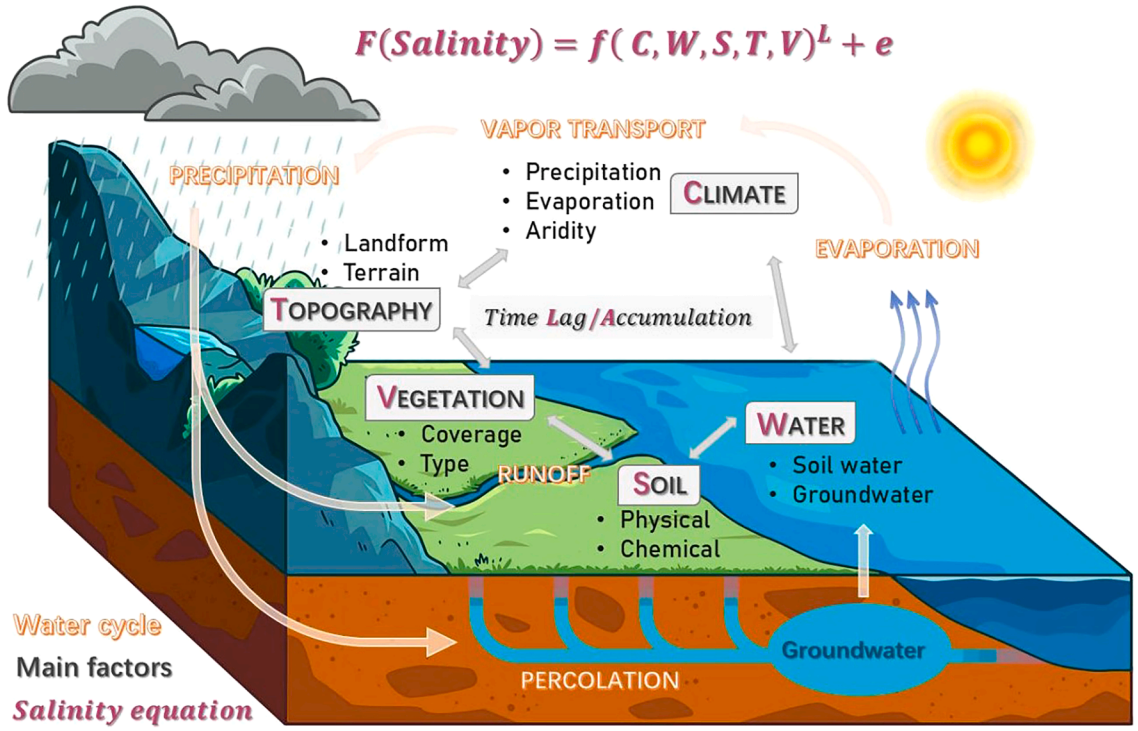

Figure 6. Soil salinization formation process

To identify soil salinity content, topography, vegetation, soil properties, and moisture conditions based on remote sensing data and geographical auxiliary data are used for quantitative estimation of time-series soil salt content. Satellite data captured and digitalized by the Moderate Resolution Imaging Spectroradiometer (MODIS) were used for estimation and mapping. MODIS imagery (i.e., specifically MOD09A1 V6.1 products) provides a long-period, freely accessible earth surface spectral reflectance of bands 1–7 at 1 km from 2000 to 2024. The MOD09A1.061 product is an ''analysis-ready'' dataset. This means that all data, for every year from 2000 to 2024, have already undergone systematic radiometric and atmospheric correction by the NASA LP DAAC using the standard MODIS Land Surface Reflectance algorithm. This algorithm corrects for the effects of gaseous absorption, Rayleigh scattering, and aerosol scattering, providing consistent surface reflectance values across the entire time series directly from GEE. No additional radiometric correction was applied by us, as the data are precorrected to a consistent standard. This means a single calibration and algorithm set was uniformly applied to the entire mission record, minimizing potential inter-annual inconsistencies due to sensor degradation or processing updates, thus ensuring the temporal consistency of our dataset across the study period (2000–2024). We then employed the ''StateQA'' (state quality assessment) band to conduct cloud and cloud shadow masking. This band contains bit flags that indicate the quality and conditions of each pixel. We used a ''0'' mask to retain only the highest-quality pixels that were clear (i.e., filtering out any pixels affected by clouds, cloud shadows, or heavy aerosols). Next, to generate cloud-free, annual representative images, we aggregated all available cloud-masked 8-day composites for each year (2000–2024). The annual value for each pixel was computed as the median of all clear-sky observations during that year. The use of the median statistic further reduces the influence of any residual atmospheric noise or outliers. This entire workflow was applied consistently across all years within GEE, ensuring methodological uniformity throughout the time series and guaranteeing a uniform methodology across the entire time period, thus ensuring the temporal consistency of our dataset.

Based on the collection time of soil verification points, the quality of remote sensing images, and the global distribution of dry seasons, we estimated salinization using remote sensing images. For each pixel, the average spectral reflectance values of images in the MODIS dataset were used to estimate the annual soil salinity content. A total of 34 indices including 20 salinity indices, two soil indices, and 12 vegetation indices were calculated based on MODIS images to be used as covariates to predict soil salinity at the global scale. The composition of soil particle size fractions (i.e., clay, silt, and sand) and topographical and geological conditions also affect the accumulation of water in soil. Soil particle size composition data were extracted from SoilGrids v.2 (250 m).[78] Groundwater table depth (WTD) data (~1 km) were obtained by compiling global observations and a groundwater mode.[79] Terrain attributes including elevation and slope were extracted from the MERIT digital elevation model (DEM; ~90 m at the equator).[80] Aridity index and potential evapotranspiration index (AI-PET), evapotranspiration (ET), and annual mean precipitation data

Table 2. Review of methodologies and covariate selections on soil salinity research employed by leading research groups

Country	Institutions	Approaches	Key attributes	Supplemental references
China	Xinjiang University, Shihezi University, CAU, CAS, CAAS, etc	remote sensing, soil experiments, soil sampling, water-salt modeling	soil properties, terrain, remote sensing (RS) bands, climate, soil moisture, groundwater, vegetation, salinity indices	Wang et al.,[55] Li et al.[66,67]
USA	USDA-ARS Salinity Laboratory	soil experiments, proximal sensing, remote sensing	soil properties, terrain, vegetation, salinity indices, soil moisture	Corwin and Lesch,[68] Scudiero et al.[69]
Australia	CSIRO, Curtin University, UNSW	long-term field trials, proximal sensing, remote sensing	soil properties, climate, vegetation, groundwater, RS bands, soil moisture	Barrett-Lennard and Qureshi,[70] Metternicht and Zinck,[71] Triantafilis et al.[72]
Portugal	Universidade de Lisboa, INIAV	proximal sensing, soil experiments	soil properties, soil moisture	Paz et al.,[73] Farzamian et al.[74]
Iran	Yazd University (affiliated with German institutions)	remote sensing, soil sampling	soil properties, terrain, climate, vegetation, RS bands, salinity indices	Fathizad et al.,[75] Taghizadeh-Mehrjardi et al.[21]
Egypt	Tanta University	remote sensing, spectroscopy, soil sampling	soil properties, terrain, climate, vegetation, salinity indices, RS bands, soil moisture	Masoud et al.[32]
Norway	Norwegian Institute for Air Research	dataset modeling	soil properties, climate, terrain, vegetation	Hassani et al.[76]
Netherlands	Wageningen University & Research	dataset modeling	soil properties	Ivushkin et al.[9]
France	Observatoire Aquitain des Sciences de l'Univers	remote sensing (radar)	soil properties, RS bands, soil moisture	Lasne et al.[77]

derived from the WorldClim 2.1 dataset (~1 km) from 2000 to 2024 were used to construct covariate datasets. A total of 42 two indices shown in Table 3 were used to construct the environmental covariate set. All data were resampled to a spatial resolution of 1 km using bilinear interpolation and spatially aligned.

Environmental hydrothermal patterns

According to soil water-salt dynamics, the salt in the soil moves with the water.[25] Specifically, annual changes in soil moisture patterns may determine the accumulation and dissolution of salt over several years.[12] We evaluated soil moisture, precipitation, soil temperature, soil evaporation, consecutive dry days, and summer days on soil salinization change. These driving factors were selected based on their established mechanistic relationships with salt accumulation processes: soil moisture and precipitation directly influence salt leaching efficiency, soil temperature affects evaporation rates and salt crystallization, while consecutive dry days and summer days represent extreme climate conditions that accelerate surface evaporation and salt concentration. The ERA5-Land Soil Moisture (SM) dataset (~11,132 m, approximately hourly temporal resolution, DOI: 10.24381/cds.e2161bac) was used to extract soil moisture patterns. The mean value of temperature, precipitation, evaporation, and water content from 2000 to 2024 of the topsoil (layer 1, 0–7 cm) was used to identify the soil moisture patterns. To explicitly link specific climate anomalies to soil salinization trends, we added two other indices: summer days (SU) and consecutive dry days (CDD). These indices are effective in characterizing the heat waves and prolonged droughts associated with extreme climate events like El Niño and record drought years.[28] These extreme climate indicators have a direct impact on evaporation and the reduction of salt leaching, which are strongly correlated with soil salinization processes. We calculated SU and CDD based on ERA5-Land data. All the hydrothermal data were calculated in GEE, and the spatial resolution was 11,132 m.

Soil salinization modeling using climate-specific RF

The climate-specific RF model was developed from classification and regression trees (CART), which is widely used for both regression and classification. Tree-based algorithms reprocess the predictions from each generated tree to ensemble a stronger learner.[81] Two parameters (ntree [the number of trees] and mtry [the number of variables in each split]) decided the largest possible size of the regression without being pruned.[78] RF is robust to multicollinearity between covariates and can automatically process various covariates to obtain a high prediction accuracy (supplemental information). Environmental covariates contribute differently to the process of soil salinity accumulation under wet/dry conditions in different climate regions. Therefore, five climate-specific RF regression models were used to train soil datasets from each climate region.[82] The number of variables at each split (mtry) was optimized from 1 to 42, and the number of trees (ntree) was optimized from 500 to 1,000 (steps of 100) to loop with the minimum root mean squared error (RMSE). To evaluate the performance of the soil salinity estimation, accuracy

Please cite this article in press as: Wang et al., Mapping 25 years of global soil salinity: Hydrothermal conditions drive widespread desalinization amid regional salinization hotspots, One Earth (2026), https://doi.org/10.1016/j.oneear.2026.101658

Table 3. Forty-two covariates based on geological axillary data and remote sensing data, with feature types, description, abbreviation, and formula

Feature types	Description	Abbreviation	Formula
Geological axillary data	groundwater table depth	WTD	–
	precipitation	Prec	–
	aridity index and potential evapotranspiration index	AI-ET	–
	evapotranspiration	ET	–
	sand content	Sand	–
	silt content	Silt	–
	clay content	Clay	–
	slope	Slope	–
Salinity indices	salinity index	SI	$(G \times R)^{0.5}$
	salinity index 1	SI1	$(G + R)^{0.5}$
	salinity index 2	SI2	$(NIR^2 + G^2 + R^2)^{0.5}$
	salinity index 3	SI3	$(G^2 + R^2)^{0.5}$
	salinity Index 4	SI4	$SWIR_1/NIR$
	salinity index I	S1	B/R
	salinity index II	S2	$(B - R)/(B + R)$
	salinity index III	S3	$G \times R/B$
	salinity index V	S5	$B \times R/G$
	salinity index VI	S6	$R \times NIR/G$
	salinity index VII	S8	$(G + R)/2$
	salinity index IX	S9	$(G + R + NIR)/2$
	salinity index	SI-T	$R/NIR \times 100$
	soil salinity and sodicity indices 1	SSSI-1	$R - NIR$
	soil salinity and sodicity indices 2	SSSI-2	$(R \times NIR - NIR \times NIR)/R$
	normalized difference salinity index	NDSI	$(NIR - SWIR_1)/(NIR + SWIR_1)$
	canopy response salinity index	CRSI	$[(NIR \times R - G \times B)/(NIR \times R + G \times B)]^{0.5}$
	salinization remote sensing index	SRSI	$[(NDVI - 1)^2 + SI^2]^{0.5}$
	salinity ratio index	SAIO	$(G - NIR)/(B + NIR)$
	enhanced residues soil salinity index	ERSSI	$G^2/(B \times SWIR_1)$
Soil indices	carbonate index	CAEX	G/B
	brightness index	BI	$(G^2 + B^2)^{0.5}$
Vegetation indices	ratio vegetation index	RVI	NIR/R
	enhanced normalized differential vegetation index	ENDVI	$(NIR + SWIR_1 - R)/(NIR + SWIR_1 + R)$
	infrared percentage vegetation index	IPVI	$NIR/(NIR + R)$
	generalized difference vegetation index	GDVI	$(NIR^2 - R^2)/(NIR^2 + R^2)$
	non-linear vegetation index	NLI	$(NIR^2 - R)/(NIR^2 + R)$
	green atmospherically resistant vegetation index	GARI	$\{NIR - [G + \gamma \times (B - R)]\}/\{NIR + [G + \gamma \times (B - R)]\}$
	normalized differential vegetation index	NDVI	$(NIR - R)/(NIR + R)$
	differential vegetation index	DVI	$NIR - R$
	enhanced vegetation index	EVI	$(1 + L) \times (NIR - R)/(NIR + C1 \times R - C2 \times B + L)$
	soil-adjusted vegetation index	SAVI	$[(NIR - R)/(NIR + R + L)] \times (1 + L)$
	optimized soil-adjusted vegetation index	OSAVI	$(NIR - R)/(NIR + R + 0.16)$
	global vegetation moisture index	GVMI	$[(NIR +0.1) - (SWIR_1 + 0.02)]/[(NIR + 0.1) + (SWIR_1 + 0.02)]$

evaluation indicators including R^2, RMSE, and Lin's concordance correlation coefficient (LCCC) were used as follows:

$$R^2 = 1 - \frac{\sum_{i=1}^{n}(y_i - \hat{y}_i)^2}{\sum_{i=1}^{n}(y_i - \bar{y})^2}, \quad \text{(Equation 2)}$$

$$\text{RMSE} = \sqrt{\frac{\sum_{i=1}^{n}((y_i - \hat{y}_i)^2}{n}}, \quad \text{(Equation 3)}$$

$$\text{LCCC} = \frac{2 \times r \times s_{Y_{model}} \times s_{Y_{testing}}}{s^2_{Y_{model}} + s^2_{Y_{testing}} + \left(\overline{Y}_{\text{model}} - \overline{Y}_{\text{testing}}\right)^2}, \quad \text{(Equation 4)}$$

where n is the number of soil samples, y_i and $\hat{y}_i$ are the observed and predicted soil EC_e value for sample i, and $\bar{y}$ is the mean of observed EC_e value. r is Pearson coefficient of measured and estimated value. $s_{Y_{model}}$ and $s_{Y_{testing}}$ are standard deviation of the estimated and measured soil EC_e value, respectively. The time-series quantitative estimation of global soil salinity using RF regression was trained and mapped in GEE.

Time-lag analysis

According to water-salt balance, the trend of hydrothermal condition change in soil has a direct interaction with the migration and accumulation of salt. Considering the effect of time lag, we define hydrothermal patterns as lagged variables. The time effect was primarily based on the established ecological concept of drought legacy effects, which operate on timescales of months to a few years. Therefore, we selected 0–5 years as the research span and calculated the trends of soil water, temperature, evaporation, precipitation, consecutive dry days, and summer days with lag effect from 0 to 5 years, respectively. Taking soil precipitation as an example, the slope of time-lag precipitation variables was defined as follows:

$$\text{Slope}_{prec,t(m)} = \frac{\sum_{i=1}^{n}(x_i - \bar{x})\left(P_{i-m} - \overline{P_{lagged}}\right)}{\sum_{i=1}^{n}(x_i - \bar{x})^2}, \quad \text{(Equation 5)}$$

where m is the lag time; n is the length of the target year sequence (n = 25 corresponds to 2000–2024); x_i is the exact year (x_1 = 2000, x_2 = 2001, …); $\bar{x}$ is the mean value of years; P_{i-m} is the precipitation with a lag of m years; and $\overline{P_{lagged}}$ is the mean value of the lagging precipitation sequence.[32] The parameters of m ranged from 0 to 5 to calculate the slope of features as the lag time of soil precipitation, evaporation, temperature, water, SU, and CDD influencing the soil salinity.

We then conducted RF regression and SHAP analysis on the hydrothermal trend and salinization by pixel (supplemental information). The pixel-by-pixel driving factor (with time effect) was obtained at 11,132 m.

TS median trend analysis and MK test

The TS median trend analysis is a robust non-parametric trend statistical method and is applied to judge the trend of long-time series data of each pixel in a time series by combining with the MK test.[83] Taking EC as an example, the slope of TS median of soil salinity between 2000 and 2024 was defined as follows:

$$\text{Slope}_{EC} = median\left(\frac{EC_j - EC_i}{j - i}\right), \quad \text{(Equation 6)}$$

where, Slope_{EC} refers to the TS median, and EC_i and EC_j represent the soil salinity content of years of i and j where $2000 \le i < j \le 2024$.

The MK test is a non-parametric method used to assess the significance of the trend identified by the TS estimator, without assuming any specific data distribution and being resistant to outliers.[64] Taking time series $\{EC_i\}$ (i = 2000, 2001, …, 2024) as an example, the MK test was calculated as follows:

$$Z = \begin{cases} \frac{S-1}{\sqrt{s(S)}}, S > 0 \\ 0, S = 0 \\ \frac{S+1}{\sqrt{s(S)}}, S < 0 \end{cases}, \quad \text{(Equation 7)}$$

$$\sum_{j=1}^{n-1}\sum_{i=j+1}^{n} sgn\left(EC_j - EC_i\right), \quad \text{(Equation 8)}$$

$$sgn\left(EC_j - EC_i\right) = \begin{cases} 1, EC_j - EC_i > 0 \\ 0, EC_j - EC_i = 0 \\ -1, EC_j - EC_i < 0 \end{cases}, \quad \text{(Equation 9)}$$

$$s(S) = \frac{n(n-1)(2n+5)}{24}, \quad \text{(Equation 10)}$$

where n is the length of the time series; $sgn(EC_j - EC_i)$ is a sign function; and the Z statistic represents a given significance level ($|Z| > \mu_{1-\alpha/2}$). A confidence level of 0.05 (α = 0.05, $|Z| > 1.96$) was used to measure the significance of the EC trend from 2000 to 2024 on pixel scale.

RESOURCE AVAILABILITY

Lead contact

Requests for further information and resources should be directed to and will be fulfilled by the lead contact, Zhou Shi (shizhou@zju.edu.cn).

Materials availability

This study did not generate new unique reagents.

Data and code availability

- The data that support the findings of this study are available on request from the lead contact upon reasonable request.
- The code and data used to produce the global soil salinity map can be accessed by registered GEE users at https://code.earthengine.google.com/c059b261b6928beab43c287efd8edea8.
- Any additional information required to reanalyze the data reported in this paper is available from the lead contact upon request.

ACKNOWLEDGMENTS

This study was supported by the National Natural Science Foundation of China (42501063 and 42261016); National Key Research and Development Program of China (2023YFD1900102).

AUTHOR CONTRIBUTIONS

N.W. and Z.S. designed the research, carried out salinity estimation, and wrote the manuscript; N.W. and D.Y. analyzed the data; S.C., A.B., F.F., and J.H. provided ideas toward method development; R.T.-M. and J.-P.W. collected soil data for model testing; J.-P.W. and F.F. evaluated the results; and all authors reviewed and edited the manuscript.

DECLARATION OF INTERESTS

The authors declare no competing interests.

SUPPLEMENTAL INFORMATION

Supplemental information can be found online at https://doi.org/10.1016/j.oneear.2026.101658.

Received: February 25, 2025
Revised: November 9, 2025
Accepted: March 10, 2026

REFERENCES

1. Lal, R. (2012). Climate change and soil degradation mitigation by sustainable management of soils and other natural resources. Agric. Res. *1*, 199–212. https://doi.org/10.1007/s40003-012-0031-9.
2. Lal, R. (2015). Restoring soil quality to mitigate soil degradation. Sustainability *7*, 5875–5895. https://doi.org/10.3390/su7055875.
3. Wang, N., Chen, S., Huang, J., Frappart, F., Taghizadeh, R., Zhang, X., Wigneron, J.-P., Xue, J., Xiao, Y., Peng, J., and Shi, Z. (2024). Global soil salinity estimation at 10 m using multi-source remote sensing. J. Remote Sens. *4*, 0130. https://doi.org/10.34133/remotesensing.0130.
4. Schofield, R.V., and Kirkby, M.J. (2003). Application of salinization indicators and initial development of potential global soil salinization scenario under climatic change. Glob. Biogeochem. Cycles *17*. https://doi.org/10.1029/2002GB001935.
5. Kaushal, S.S., Likens, G.E., Mayer, P.M., Shatkay, R.R., Shelton, S.A., Grant, S.B., Utz, R.M., Yaculak, A.M., Maas, C.M., Reimer, J.E., et al. (2023). The anthropogenic salt cycle. Nat. Rev. Earth Environ. *4*, 770–784. https://doi.org/10.1038/s43017-023-00485-y.
6. Kiliç, K., and Kiliç, S. (2007). Spatial variability of salinity and alkalinity of a field having salination risk in semi-arid climate in northern Turkey. Environ. Monit. Assess. *127*, 55–65. https://doi.org/10.1007/s10661-006-9258-x.
7. Khasanov, S., Kulmatov, R., Li, F., van Amstel, A., Bartholomeus, H., Aslanov, I., Sultonov, K., Kholov, N., Liu, H., and Chen, G. (2023). Impact assessment of soil salinity on crop production in Uzbekistan and its global significance. Agric. Ecosyst. Environ. *342*, 108262. https://doi.org/10.1016/j.agee.2022.108262.
8. Turek, M.E., Poggio, L., Batjes, N.H., Armindo, R.A., de Jong van Lier, Q., de Sousa, L., and Heuvelink, G.B. (2023). Global mapping of volumetric water retention at 100, 330 and 15 000 cm suction using the WoSIS database. Int. Soil Water Conserv. Res. *11*, 225–239. https://doi.org/10.1016/j.iswcr.2022.08.001.
9. Ivushkin, K., Bartholomeus, H., Bregt, A.K., Pulatov, A., Kempen, B., and de Sousa, L. (2019). Global mapping of soil salinity change. Remote Sens. Environ. *231*, 111260. https://doi.org/10.1016/j.rse.2019.111260.
10. Várallyay, G., Climate change, soil salinity and alkalinity. Soil Responses to Climate Change. NATO ASI Series, vol 23. Springer, Berlin, Heidelberg. https://doi.org/10.1007/978-3-642-79218-2_4.
11. Racetin, I., Krtalic, A., Srzic, V., and Zovko, M. (2020). Characterization of short-term salinity fluctuations in the Neretva River Delta situated in the southern Adriatic Croatia using Landsat-5 TM. Ecol. Indic. *110*, 105924. https://doi.org/10.1016/j.ecolind.2019.105924.
12. Eswar, D., Karuppusamy, R., and Chellamuthu, S. (2021). Drivers of soil salinity and their correlation with climate change. Curr. Opin. Environ. Sustain. *50*, 310–318. https://doi.org/10.1016/j.cosust.2020.10.015.
13. Kawser, U., Nath, B., and Hoque, A. (2022). Observing the influences of climatic and environmental variability over soil salinity changes in the Noakhali Coastal Regions of Bangladesh using geospatial and statistical techniques. Environ. Chall. *6*, 100429. https://doi.org/10.1016/j.envc.2021.100429.
14. Bannari, A., and Al-Ali, Z.M. (2020). Assessing climate change impact on soil salinity dynamics between 1987–2017 in arid landscape using Landsat TM, ETM+ and OLI data. Remote Sens. *12*, 2794. https://doi.org/10.3390/rs12172794.
15. Corwin, D.L. (2020). Climate change impacts on soil salinity in agricultural areas. Eur. J. Soil Sci. *72*, 842–862. https://doi.org/10.1111/ejss.13010.
16. Thorslund, J., Bierkens, M.F.P., Oude Essink, G.H.P., Sutanudjaja, E.H., and van Vliet, M.T.H. (2021). Common irrigation drivers of freshwater salinisation in river basins worldwide. Nat. Commun. *12*, 4232. https://doi.org/10.1038/s41467-021-24281-8.
17. Menke, W., and Menke, J. (2016). Data analysis with MatLab. Environmental Data Analysis with MATLAB (Academic Press), pp. 1–19.
18. Begum, B., Tajbar, S., Khan, B., and Rafiq, L. (2021). Identification of relationships between climate indices and precipitation fluctuation in Peshawar City-Pakistan. J. Res. Environ. Earth Sci. *10*, 264–278.
19. Khosravichenar, A., Aalijahan, M., Moaazeni, S., Lupo, A.R., Karimi, A., Ulrich, M., Parvian, N., Sadeghi, A., and von Suchodoletz, H. (2023). Assessing a multi-method approach for dryland soil salinization with respect to climate change and global warming – The example of the Bajestan region (NE Iran). Ecol. Indic. *154*, 110639. https://doi.org/10.1016/j.ecolind.2023.110639.
20. Gorji, T., Yildirim, A., Hamzehpour, N., Tanik, A., and Sertel, E. (2020). Soil salinity analysis of Urmia Lake Basin using Landsat-8 OLI and Sentinel-2A based spectral indices and electrical conductivity measurements. Ecol. Indic. *112*, 106173. https://doi.org/10.1016/j.ecolind.2020.106173.
21. Taghizadeh-Mehrjardi, R., Schmidt, K., Toomanian, N., Heung, B., Behrens, T., Mosavi, A., S. Band, S., Amirian-Chakan, A., Fathabadi, A., and Scholten, T. (2021). Improving the spatial prediction of soil salinity in arid regions using wavelet transformation and support vector regression models. Geoderma *383*, 114793. https://doi.org/10.1016/j.geoderma.2020.114793.
22. Alhammadi, M.S., and Glenn, E.P. (2008). Detecting date palm trees health and vegetation greenness change on the eastern coast of the United Arab Emirates using SAVI. Int. J. Remote Sens. *29*, 1745–1765. https://doi.org/10.1080/01431160701395195.
23. Taghadosi, M.M., and Hasanlou, M. (2017). Trend analysis of soil salinity in different land cover types using Landsat time series data-case study Bakhtegan Salt Lake. Int. Arch. Photogramm. Remote Sens. Spatial Inf. Sci. *42*, 251–257. https://doi.org/10.5194/isprs-archives-XLII-4-W4-251-2017.
24. Peng, J., Biswas, A., Jiang, Q., Zhao, R., Hu, J., Hu, B., and Shi, Z. (2019). Estimating soil salinity from remote sensing and terrain data in southern Xinjiang Province, China. Geoderma *337*, 1309–1319. https://doi.org/10.1016/j.geoderma.2018.08.006.
25. Han, L., Liu, D., Cheng, G., Zhang, G., and Wang, L. (2019). Spatial distribution and genesis of salt on the saline playa at Qehan Lake, Inner Mongolia, China. Catena *177*, 22–30. https://doi.org/10.1016/j.catena.2019.01.040.
26. Bhuyan, M.I., Mia, S., Supit, I., and Ludwig, F. (2023). Spatio-temporal variability in soil and water salinity in the south-central coast of Bangladesh. Catena *222*, 106786. https://doi.org/10.1016/j.catena.2022.106786.
27. Dasgupta, S., Hossain, M.M., Huq, M., and Wheeler, D. (2015). Climate change and soil salinity: The case of coastal Bangladesh. Ambio *44*, 815–826. https://doi.org/10.1007/s13280-015-0681-5.

28. Valdivia-Silva, J.E., Navarro-González, R., Fletcher, L., Pérez-Montaño, S., Condori-Apaza, R., Ortega-Gutiérrez, F., and McKay, C. (2012). Climatological characteristics in the extreme hyper-arid region of Pampas de La Joya, Peru. Astrobiological approach in four years of observation: 2004–2008. Int. J. Astrobiol. *11*, 25–35. https://doi.org/10.1017/S1473550411000292.

29. Alfarrah, N., and Walraevens, K. (2018). Groundwater overexploitation and seawater intrusion in coastal areas of arid and semi-arid regions. Water *10*, 143. https://doi.org/10.3390/w10020143.

30. Frappart, F. (2020). Groundwater storage changes in the major North African transboundary aquifer systems during the GRACE era (2003–2016). Water *12*, 2669. https://doi.org/10.3390/w12102669.

31. Etemad-Shahidi, A., Parsa, J., and Hajiani, M. (2011). Salinity intrusion length: comparison of different approaches. In Proceedings of the Institution of Civil Engineers-Maritime Engineering (Thomas Telford Ltd), pp. 33–42. https://doi.org/10.1680/maen.2011.164.1.33.

32. Masoud, A.A., Koike, K., Atwia, M.G., El-Horiny, M.M., and Gemail, K.S. (2019). Mapping soil salinity using spectral mixture analysis of Landsat 8 OLI images to identify factors influencing salinization in an arid region. Int. J. Appl. Earth Obs. Geoinf. *83*, 101944. https://doi.org/10.1016/j.jag.2019.101944.

33. Alexakis, D.D., Daliakopoulos, I.N., Panagea, I.S., and Tsanis, I.K. (2016). Assessing soil salinity using WorldView-2 multispectral images in Timpaki, Crete, Greece. Geocarto Int. *33*, 321–338. https://doi.org/10.1080/10106049.2016.1250826.

34. Alber, M., Swenson, E.M., Adamowicz, S.C., and Mendelssohn, I.A. (2008). Salt Marsh Dieback: An overview of recent events in the US. Estuar. Coast. Shelf Sci. *80*, 1–11. https://doi.org/10.1016/j.ecss.2008.08.009.

35. Lopes, C.L., Mendes, R., Caçador, I., and Dias, J.M. (2020). Assessing salt marsh extent and condition changes with 35 years of Landsat imagery: Tagus Estuary case study. Remote Sens. Environ. *247*, 111939. https://doi.org/10.1016/j.rse.2020.111939.

36. Müller, L.M., and Bahn, M. (2022). Drought legacies and ecosystem responses to subsequent drought. Glob. Change Biol. *28*, 5086–5103. https://doi.org/10.1111/gcb.16270.

37. Han, L., Ding, J., Zhang, J., Chen, P., Wang, J., Wang, Y., Wang, J., Ge, X., and Zhang, Z. (2021). Precipitation events determine the spatiotemporal distribution of playa surface salinity in arid regions: evidence from satellite data fused via the enhanced spatial and temporal adaptive reflectance fusion model. Catena *206*, 105546. https://doi.org/10.1016/j.catena.2021.105546.

38. Bi, W.P., Lin, D., and Mao, X.M. (2024). Two-dimensional transport patterns of soil water, heat and salt under mulched drip irrigation with brackish water in cotton fields of Southern Xinjiang and the optimal irrigation schedule. Trans. Chin. Soc. Agric. Eng. *40*, 155–168. (in Chinese). https://doi.org/10.11975/j.issn.1002-6819.202404034.

39. Liu, B., Wang, S., Liu, X., and Sun, H. (2022). Evaluating soil water and salt transport in response to varied rainfall events and hydrological years under brackish water irrigation in the North China Plain. Geoderma *422*, 115954. https://doi.org/10.1016/j.geoderma.2022.115954.

40. Corwin, D.L., Rhoades, J.D., and Šimůnek, J. (2007). Leaching requirement for soil salinity control: Steady-state versus transient models. Agric. Water Manag. *90*, 165–180. https://doi.org/10.1016/j.agwat.2007.02.007.

41. Rengasamy, P. (2021). Climate change impacts on soil salinity in agricultural areas. Eur. J. Soil Sci. *72*, 842–862. https://doi.org/10.1111/ejss.13010.

42. IPCC (2019). In Climate Change and Land: an IPCC special report on climate change, desertification, land degradation, sustainable land management, food security, and greenhouse gas fluxes in terrestrial ecosystems, P.R. Shukla, J. Skea, E. Calvo Buendia, V. Masson-Delmotte, H.-O. Pörtner, D.C. Roberts, P. Zhai, R. Slade, S. Connors, and R. van Diemen, et al., eds. (IPCC).

43. Akram, M., Kahlown, M.A., and Soomro, Z.A. (2008). Desertification Control for Sustainable Land Use in the Cholistan Desert, Pakistan. In The Future of Drylands, C. Lee and T. Schaaf, eds. (Springer). https://doi.org/10.1007/978-1-4020-6970-3_44.

44. Fatima, B., Ashraf, M., Ahmad, A., and Hasan, F.U. (2021). Integrated Water Resources Management, Implementation Guidelines for Pakistan (Pakistan Council of Research in Water Resources). In The Future of Drylands: International Scientific Conference on Desertification and Drylands Research Tunis, Tunisia, 19-21 June 2006 (Springer Netherlands). https://doi.org/10.1007/978-1-4020-6970-3_44.

45. De la Fuente, G.,M.C., Allende, C.,M., and Calle, Z.,I. (2020). INIA Ururi 13 años trabajando por el desarrollo agropecuario sostenible de la región de Arica y Parinacota. In Informe de Gestión y Evaluación de Tecnologías (2006-2019) https://hdl.handle.net/20.500.14001/68068.

46. Eyl-Mazzega, M.-A., and Cassignol, E. (2022). The Geopolitics of Seawater Desalination (Institut Français des Relations Internationales).

47. Food and Agriculture Organization of the United Nations (FAO) (2021). Global Map of Salt-Affected Soils (GSASmap) (Food and Agriculture Organization of the United Nations (FAO)). https://www.fao.org/soils-portal/data-hub/soil-maps-and-databases/global-map-of-salt-affected-soils/en/.

48. Hassani, A., Azapagic, A., and Shokri, N. (2021). Global predictions of primary soil salinization under changing climate in the 21st century. Nat. Commun. *12*, 6663. https://doi.org/10.1038/s41467-021-26907-3.

49. FAO (2021). Handbook for Saline Soil Management (FAO). https://openknowledge.fao.org/handle/20.500.14283/i7318en.

50. Toderich, K.N., Bobokulov, N.A., Rabbimov, A.P., Shuiskaya, E.V., Mukimov, T.K., Popova, V.V., and Khakimov, U.N. (2015). Kochia prostrata (L) Schrad – valuable fodder crop that improves pasture quality in desert and semidesert areas (Research Monograph). (in Russian). 146 стр. ISBN 978–9943–975–41–5.

51. S.A. Balyuk, R.S. Truskavetsky, and Y.L. Tsapko, eds. (2012). Chemical Amelioration of Grounds (Innovation Development Concept) [in Ukrainian] (Miskdruk) http://www.eolss.net/Eolss-sampleAllChapter.aspx.

52. Chen, S., Arrouays, D., Mulder, V.L., Poggio, L., Minasny, B., Roudier, P., Libohova, Z., Lagacherie, P., Shi, Z., Hannam, J., et al. (2022). Digital mapping of soil properties at a broad scale: A review. Geoderma *409*, 115567. https://doi.org/10.1016/j.geoderma.2021.115567.

53. Fick, S.E., and Hijmans, R.J. (2017). WorldClim 2: new 1-km spatial resolution climate surfaces for global land areas. Int. J. Climatol. *37*, 4302–4315. https://doi.org/10.1002/joc.5086.

54. Hartmann, J., and Moosdorf, N. (2012). The new global lithological map database GLiM: A representation of rock properties at the Earth surface. Geochem. Geophys. Geosyst. *13*. https://doi.org/10.1029/2012GC004370.

55. Wang, J., Ding, J., Yu, D., Teng, D., He, B., Chen, X., Ge, X., Zhang, Z., Wang, Y., Yang, X., et al. (2020). Machine learning-based detection of soil salinity in an arid desert region, Northwest China: A comparison between Landsat-8 OLI and Sentinel-2 MSI. Sci. Total Environ. *707*, 136092. https://doi.org/10.1016/j.scitotenv.2019.136092.

56. Wadoux, A.M.J.C., Minasny, B., and McBratney, A.B. (2020). Machine learning for digital soil mapping: Applications, challenges and suggested solutions. Earth Sci. Rev. *210*, 103359. https://doi.org/10.1016/j.earscirev.2020.103359.

57. Peel, M.C., Finlayson, B.L., and McMahon, T.A. (2007). Updated world map of the Köppen-Geiger climate classification. Hydrol. Earth Syst. Sci. *11*, 1633–1644. https://doi.org/10.5194/hess-11-1633-2007.

58. Murray, N.J., Phinn, S.R., DeWitt, M., Ferrari, R., Johnston, R., Lyons, M.B., Clinton, N., Thau, D., and Fuller, R.A. (2019). The global distribution and trajectory of tidal flats. Nature *565*, 222–225. https://doi.org/10.1038/s41586-018-0805-8.

59. Tellman, B., Sullivan, J.A., Kuhn, C., Kettner, A.J., Doyle, C.S., Brakenridge, G.R., Erickson, T.A., and Slayback, D.A. (2021). Satellite imaging reveals increased proportion of population exposed to floods. Nature *596*, 80–86. https://doi.org/10.1038/s41586-021-03695-w.

60. Trabucco, A., and Zomer, R.J. (2018). Global Aridity Index and Potential Evapo-Transpiration (ET0) Climate Database v2. https://doi.org/10.6084/m9.figshare.7504448.v2.

61. Batjes, N.H., Ribeiro, E., and van Oostrum, A. (2019). Standardised soil profile data for the world (WoSIS Snapshot – September 2019). https://doi.org/10.17027/isric-wdcsoils.20190901.

62. Rhoades, J.D. (1982). Soluble Salts. In Handbook of Soil Analysis (Springer), pp. 167–179. https://doi.org/10.1007/978-3-540-31211-6_18.

63. Ren, F., Yang, G., Li, W., He, X., Gao, Y., Tian, L., Li, F., Wang, Z., and Liu, S. (2021). Yield-compatible salinity level for growing cotton (Gossypium hirsutum L.) under mulched drip irrigation using saline water. Agric. Water Manag. *250*, 106859. https://doi.org/10.1016/j.agwat.2021.106859.

64. Wang, X., Zhang, F., Kung, H.-T., Johnson, V.C., and Latif, A. (2019). Extracting soil salinization information with a fractional-order filtering algorithm and grid-search support vector machine (GS-SVM) model. Int. J. Remote Sens. *41*, 953–973. https://doi.org/10.1080/01431161.2019.1654142.

65. Li, Y., Li, Z., Gong, P., He, X., Liu, H., Li, L., Wang, C., Li, P., Wei, J., and Yu, X. (2024). Enhanced irrigation volume reduces salinity and improves deep root zone soil nutrients, phosphatase activity and changes root traits of fruit trees. Agric. Water Manag. *302*, 109001. https://doi.org/10.1016/j.agwat.2024.109001.

66. Li, Y., Gong, P., He, X., Liu, H., Li, Z., Li, L., Wang, C., Xu, Q., Chen, Q., Wei, J., Lin, P., and Yu, X. (2024). Simulating water and salt changes in the root zone of salt-alkali fragrant pear and the selection of the optimal surface drip irrigation mode. Front. Plant Sci. *15*, 1455188. https://doi.org/10.3389/fpls.2024.1455188.

67. Li, H.Q., Yao, R.J., Yang, J.S., Wang, X.P., Xie, W.P., and Zhang, L. (2020). Mechanisms of the effects of salinization on nitrogen transformation in farmland and pathways for enhanced efficiency regulation. Chin. J. Appl. Ecol. *31*, 3847–3856. (in Chinese). https://doi.org/10.13287/j.1001-9332.202011.023.

68. Corwin, D.L., and Lesch, S.M. (2005). Apparent soil electrical conductivity measurements in agriculture. Comput. Electron. Agric. *46*, 11–43. https://doi.org/10.1016/j.compag.2004.10.005.

69. Scudiero, E., Skaggs, T.H., and Corwin, D.L. (2014). Regional scale soil salinity evaluation using Landsat 7, western San Joaquin Valley, California, USA. Geoderma Reg *2–3*, 82–90. https://doi.org/10.1016/j.geodrs.2014.10.004.

70. Barrett-Lennard, E.G., and Qureshi, R.H. (1997). Saline agriculture for irrigated land in Pakistan: A handbook. ACIAR Monograph No, *142* (Australian Centre for International Agricultural Research).

71. Metternicht, G.I., and Zinck, J.A. (2003). Remote sensing of soil salinity: potentials and constraints. Remote Sens. Environ. *85*, 1–20. https://doi.org/10.1016/S0034-4257(02)00188-8.

72. Triantafilis, J., Odeh, I.O.A., Minasny, B., and McBratney, A.B. (2003). Elucidation of physiographic and hydrogeological features of the lower Namoi valley using fuzzy k-means classification of EM34 data. Environ. Model. Softw. *18*, 667–680. https://doi.org/10.1016/S1364-8152(03)00053-7.

73. Paz, A.M., Castanheira, N., Farzamian, M., Paz, M.C., Gonçalves, M.C., Monteiro Santos, F.A., and Triantafilis, J. (2020). Prediction of soil salinity and sodicity using electromagnetic conductivity imaging. Geoderma 361, 114086. 10.1016/j.geoderma.2019.114086.

74. Farzamian, M., Paz, M.C., Paz, A.M., Castanheira, N.L., Gonçalves, M.C., Monteiro Santos, F.A., and Triantafilis, J. (2019). Mapping soil salinity using electromagnetic conductivity imaging—A comparison of regional and location-specific calibrations. Land Degrad. Dev. 30, 1393–1406. 10.1002/ldr.3317.

75. Fathizad, H., Hakimzadeh Ardakani, M.A., Sodaiezadeh, H., Kerry, R., and Taghizadeh-Mehrjardi, R. (2020). Investigation of the spatial and temporal variation of soil salinity using random forests in the central desert of Iran. Geoderma *365*, 114233. https://doi.org/10.1016/j.geoderma.2020.114233.

76. Hassani, A., Azapagic, A., and Shokri, N. (2020). Predicting long-term dynamics of soil salinity and sodicity on a global scale. Proc. Natl. Acad. Sci. USA *117*, 33017–33027. https://doi.org/10.1073/pnas.2013771117.

77. Lasne, Y., Paillou, P., Ruffle, G., Serradilla, C., Demontoux, F., Freeman, A., Farr, T., McDonald, K., Chapman, B., and Malezieux, J.-M. (2007). Effect of salinity on the dielectric properties of geological materials: implication for soil moisture detection by means of remote sensing. In 2007 IEEE International Geoscience and Remote Sensing Symposium (IEEE), pp. 3689–3693. https://doi.org/10.1109/IGARSS.2007.4423644.

78. Poggio, L., De Sousa, L.M., Batjes, N.H., Heuvelink, G.B.M., Kempen, B., Ribeiro, E., and Rossiter, D. (2021). SoilGrids 2.0: producing soil information for the globe with quantified spatial uncertainty. Soil *7*, 217–240. https://doi.org/10.5194/soil-7-217-2021.

79. Fan, Y., Li, H., and Miguez-Macho, G. (2013). Global Patterns of Groundwater Table Depth. Science *339*, 940–943. https://doi.org/10.1126/science.1229881.

80. Yamazaki, D., Ikeshima, D., Tawatari, R., Yamaguchi, T., O'Loughlin, F., Neal, J.C., Sampson, C.C., Kanae, S., and Bates, P.D. (2017). A high-accuracy map of global terrain elevations. Geophys. Res. Lett. *44*, 5844–5853. https://doi.org/10.1002/2017GL072874.

81. Breiman, L. (2001). Random forests. Mach. Learn. *45*, 5–32. https://doi.org/10.1023/A:1010933404324.

82. Ma, M., Wang, Q., Liu, R., Zhao, Y., and Zhang, D. (2023). Effects of climate change and human activities on vegetation coverage change in northern China considering extreme climate and time-lag and -accumulation effects. Sci. Total Environ. *860*, 160527. https://doi.org/10.1016/j.scitotenv.2022.160527.

83. Sen, P.K. (1968). Estimates of the regression coefficient based on Kendall's tau. J. Am. Stat. Assoc. *63*, 1379–1389. https://doi.org/10.1080/01621459.1968.10480934.